Cyanobacterial spheroids and other biosignatures from microdigitate stromatolites of Mesoproterozoic Wumishan Formation in Jixian, North China

Hao Yang[1], Zhong-Qiang Chen[1] *, Dominic Papineau[1, 2]
[1]State Key Laboratory of Biogeology and Environmental Geology, China University of Geosciences (Wuhan), Wuhan 430074, China
[2]Department of Earth Sciences, London Centre for Nanotechnology & Centre for Planetary Sciences, University College London, WC1H 0AH, UK

*Corresponding author. E-mail address: zhong.qiang.chen@cug.edu.cn (Z.-Q. Chen)

Abstract

Stromatolites have been widely reported from the Archean and Paleoproterozoic successions worldwide, and they could represent one of oldest life forms on Earth. Of these, a group of small stromatolites occur as microdigitate low-relief columns, and are also conspicuous in the field. However, biogenicity of these microdigitate stromatolites (MDSs) has long been disputed due to to the abundance of radial-fibrous texture and a lack of convincing microfossils. New examples of MDS are documented from the Mesoproterozoic Wumishan Formation of the Jixian area, North China. Vertically oriented fibrous fabrics are conspicuous and penetrate laminae as well as microscopic spheroids, which point to an abiotic genesis for this specific fabric. Stromatolite laminae contain abundant spheroids, typically 15–30 μm in diameter, with single or double outlines and they occur as solitary coccoid-like microfossils or in small aggregated colonies. Spheroids show strong fluorescence under both green and purple exciting lights, consistent with their composition of organic matter. Spheroids are abundant in the Wumishan stromatolites and they are categorized into two types. The first kind comprises micrite nuclei surrounded by sparitic sheaths, without nano-particle coatings. A smooth to grainy spheroidal surface defines the first kind of spheroids that also has a distinct rounded opening, which is often broken probably due to diagenesis and silicification. The second kind of spheroids is usually

covered with nano-particles and lacks circular opening on surface. These spheroids possess large nuclei of single sparitic calcite coated with thin sparry sheaths. Overall, the Wumishan spheroids resemble coccoidal microorganisms reported from other Archean-Paleoproterozoic strata worldwide, but they are also better preserved. The rounded opening on spheroid surface is interpreted as division point of unicells during reproduction of the life cycle of bacteria akin to *Myxococcoides grandis*. Clump-like micro-particle aggregates in nuclei could represent daughter cells released from the parental envelope, similar to the reproduction process and life cycle suggested for similar spheroidal microfossils from other similar Precambrian occurrences. The Wumishan spheroids therefore may represent fossilized prokaryotes that could have contributed to construct the MDS. Moreover, filamentous microfossils are occasionally present in the coloumns of stromatolites, and they resemble filamentous cyanobacteria, but may not be major constructors of MDS due to their rarity in the buildups. Three types of nano-particles are also conspicuous: (1) putative organic relics, such as fragmented filaments and mucuslike biofilms (purported EPS), (2) organominerals, including nanoglobules, polyhedrons, and their aggregates, and (3) dumbbell-shaped nano-particle aggregates. All of these nano-particles are interpreted to be likely biogenic in origin, and many of them were found from the radial-fibrous fabrics of carbonate precipitates in the MDS, implying that some heterotrophic bacteria may have affiliated the precipitation of radial fibers in deep-time radial-fibrous carbonate precipitates. Therefore, abundant and diverse biosignatures (spheroids, tubular filaments, and nano-particles) are identified in the Wumishan MDSs, and we conclude that diverse filamentous and coccoidal micro-organismscontributed to the formation of the Wumishan stromatolites.

Keywords: Microdigitate stromatolite, coccoid-like spheroids, nano-particles, Mesoproterozoic, North China

1. Introduction

As a laminated microbial deposit, stromatolite is the most commonly recognized life form in marine ecosystems during the first 2.5 billion years of Earth history and during a surge of abundance and morphological diversity between 1.6–1.0 Ga (Awramik, 1971, 2006; Awramik and Margulis, 1974; Awramik and Sprinkle, 1999; Allwood et al., 2006; Kah and Riding, 2007; Shi et al., 2008; Knoll, 2013; Noffke and Awramik, 2013; Tang et al., 2013a, b; Riding et al., 2014; Fralick and Riding, 2015; Tosti and Riding, 2017; Qu et al., 2018; Riding and Virgone, 2020; Baumgartner et al., 2020; Wang et al., 2021). The early stromatolites experienced a stepwise decline in abundance from the Mesoproterozoic to Neoproterozoic and reached the lowest abundance in the end of the Neoproterozoic probably due to frozen climatic regime of the snowball Earth climate during that epoch (Awramik and Sprinkle, 1999; Noffke and Awramik, 2013; Chen et al., 2019). The most pronounced evolutionary turnover of early stromatolites is the major switch from microdigitate stromatolites (MDSs) to carbonate mega-stromatolites during the Mesoproterozoic (James et al., 1998). The MDSs are perhaps one of the most morphologically distinct groups among deep time stromatolites. These stromoatolites proliferated in Neoarchean to Paleoproterozoic (>1.6 Ga), but declined significantly in Meso- and Neoproterozoic (<1.6 Ga) (Grotzinger and Knoll, 1999). MDS depletion coupled with proliferation of carbonate mega-stromatolites coincided with abundance and diversity peaks of all stromatolites in 1.6–1.0 Ga (Awramik and Sprinkle, 1999; Noffke and Awramik, 2013). Rise and demise of MDSs therefore are crucial in understanding early evolution of stromatolites.

However, genesis of MDS has long been disputed due to the abundance of radial-fibrous texture and a lack of convincing microfossils (Grotzinger and Reed, 1983; Hofmann and Jackson, 1987; Knoll et al., 1993; Sergeev et al., 1995; Grotzinger and Knoll, 1999; Riding, 2008; Riding and Virgone, 2020). Radial-fibrous textures are usually interpreted as abiotic acicular aragonite precursors that indicate calcium carbonate saturation of surface seawater (Grotzinger and Knoll, 1999; Riding and Virgone, 2020). Such radial fibers are very common in seafloor precipitates (i.e. aragonite crystal fans) that characterize the Neoarchean to Paleoproterozoic (>1.6 Ga)

carbonate successions worldwide (Grotzinger and Knoll, 1999). As abiotic processes can contribute to form these circularly concentric and radial patterns, an abiotic carbonate precipitation scenario is plausible for the accretion of MDSs (Grotzinger and Reed, 1983; Hofmann and Jackson, 1987; Knoll et al., 1993; Sergeev et al., 1995; Grotzinger and Knoll, 1999; Riding, 2008), although heterotrophic bacterial metabolism may have facilitated carbonate precipitation and nucleation during MDS formation (Knoll and Semikhatov, 1998). However, the ultrastructures of such radial-fibrous textures in carbonate precipitates have been rarely uncovered, although their microstructures are often observed under optical microscopes. Thus, whether some bacteria have involved in facilitating the precipitation of radial fibers in carbonate settings remains poorly understood.

Moreover, some Paleoproterozoic MDSs preserve successive layers of botryoidal quartz, which have been interpreted as evidence for chemically oscillating reaction during the oxidation of biomass during organic diagenesis (Goodwin and Papineau, 2021). Botryoidal malachite carbonate can also produce abiotic stromatolite-like morphologies such as turbinate and columnar (Papineau, 2020). In general, however, stromatolites are generally interpreted as biogenic in origin, and their occurrences in Paleo- and Eoarchean (3.2 to 3.8 Ga) could represent some of the oldest forms of life on Earth (Hofmann, 2000; Allwood et al., 2006; Altermann et al., 2006; Schopf et al., 2007; Noffke and Awramik, 2013; Nutman et al., 2016; Qu et al., 2018; Baumgartner et al., 2020). This is because modern and ancient stromatolites have formed through repetitive accretion of microbial mats, their precipitates, and/or entrapped inorganic materials (Riding, 2000; Dupraz et al., 2009).

The general picture of the transition from MDSs to mega-stromatolites abundance in strata is well recorded in the Mesoproterozoic successions of North China, which are well-exposed in the Jixian area of Tianjin City. In the exposed succession there, which is up to 10 km thick, the geobiological record is among the best-preserved from this period in China (Fig. 1). Stromatolites are also extremely abundant and exceptionally preserved, but concentrate mainly in two units, the Wumishan Formation and Tieling Formation, apart nearly 1000 m from one another,

at the lower and upper parts of the Mesoproterozoic succession, respectively, although they also occur sporadically in other horizons (Zhu et al., 1994; Zhang et al., 1984; Seong-Joo and Golubic, 1998, 1999; Shi et al., 2008; Tosti and Riding, 2017; Fig. 1). The Wumishan stromatolite assemblage is characterized by MDSs that have low-relief columns, while the Tieling stromatolite assemblage contains massive, branching, high-relief columnar and domal forms (Zhu et al., 1994).

The Wumishan Formation is one of the most widespread Mesoproterozoic unit in North China (Zhu et al., 1994). Abundant coccoids assignable to *Myxococcoides grandis*, after Horodyski and Donaldson (1980), have been described from cherty laminar limestone in this formation, and they were interpreted as the subsidiary mat-builders or mat-dwellers (Zhang, 1984, 1985). Stromatolites are also commonly present in the Wumishan Formation, and numerous examples from different localities have long been described in terms of mega-structures and morphology (Liang et al., 1984; Qiu and Liang, 1993; Mei et al., 2008), but little has been published on their geobiologic features and biogenicity (Tang et al., 2013b). These nanometer-scale ultrastructures were interpreted as the product of microbial activity, which are similar to the organomineral ultrastructures observed in experimental cultures (e.g., van Lith et al., 2003) and in modern mineralized microbial mats (e.g., Glunk et al., 2011). However, the builders of MDS and biogenicity of microfabrics still remain enigmatic. In addition, all Wumishan MDS are partly silicified, which could have promoted exceptional preservation of microbial structures therein as seen elsewhere (Schopf et al., 2007; Seong-Joo and Golubic, 1998, 1999; Kremer et al., 2012; Chen et al., 2014). Accordingly, this study aims to document detailed geobiological features and biosignatures in macro- to microstructures from the silicified MDS of the Wumishan Formation to provide insights to evaluate their biogenicity.

2. Geological background

The carbonate-dominated sedimentary formation was deposited in a rift basin in the North China Craton synkinematically with the break-up of Columbia and the

153 subsequent assembly of Rodinia during the Mesoproterozoic (Tang et al., 2013b; Wan
154 et al., 2015). The Mesoproterozoic succession is composed of part of the Changcheng
155 and the whole Jixian groups. The former includes the Tuanshanzi, Dahongyu, and
156 Gaoyuzhuang formations, while the Jixian Group comprises the Yangzhuang,
157 Wumishan, Hongshuizhuang, and Tieling formations (Zhu et al., 1994; Fig. 1). This
158 Mesoproterozoic succession is well exposed in Jixian area, which is situated along the
159 northeastern margin of the North China Craton.

160 The described MDS was collected from the lower Wumishan Formation in the
161 Mopanyu section (GPS: 40°9.131′N; 117°23.740′E) of Luozhuangzi Town, Jixian
162 County, near Tianjin City in North China (Fig. 1). At this locality, the Wumishan
163 Formation succession is exposed in road cuts along the Jixian-Luozhuangzi highway.
164 This formation is in conformable contact with the underlying Yangzhuang Formation
165 and with the overlying Hongshuizhuang Formation (Zhu et al., 1994). Lithologically,
166 the Wumishan Formation, up to 3336 m in thickness, is characterized by alternations
167 of dolomite and limestone. The entire formation appears rhythmically banded.
168 Microbialites include both stromatolites and thrombolites, which usually occur in the
169 thicker parts of the parasequence (Mei et al., 2008; Tang et al., 2013a, b).

170 The Wumishan Formation is subdivided into four members (Chen et al., 1980).
171 Of these, Member 1 is mainly composed of laminated dolostones interbedded with
172 calcareous shales, and thrombolites and cherty bands. This member was likely
173 deposited in the lower to upper parts of subtidal zone of shallow platform setting.
174 Member 2 is dominated by massive laminated dolostones and thrombolitic dolostones
175 which are interpreted to be deposited in upper subtidal to intertidal settings. Member 3
176 is characterized by thick-bedded thrombolitic and laminated dolostones, which were
177 likely deposited in lower subtidal to lower intertidal settings. Member 4 is comprised
178 of medium-bedded, laminated and micritic dolostones of upper subtidal to intertidal
179 facies (Shi et al. 2008). Overall, this formation was deposited in subtidal to peritidal
180 environments on a shallow carbonate platform (Mei et al., 2001, 2010; Zhou et al.,
181 2006; Shi et al., 2008; Shi and Jiang, 2011; Tang et al., 2011). Cherty bands and
182 nodules are commonly present in thinly laminated, peritidal dolostone. The studied

MDS occurs in the thicker unit of cyclic sequences in Member 1 (Zhu et al., 1978; Zhu, 1982; Liang, 1984; Zhu and Liang, 1993; Fig. 2). The MDS-bearing strata of Member 1 comprise thin-bedded, laminated dolomites, thick-bedded dolostone, and calcareous dolomitic shales (Fig. 2). Meter-thick depositional cycles are conspicuous in the field, and each cycle comprises calcareous shales or thin-bedded laminated dolostone in the lower part, and relatively thick-bedded thrombolitic or stromatolitic or laminated dolomites in the upper part (Fig. 2). The lower units were usually deposited in lower part of subtidal (LST) zone, while the upper units were usually interpreted as the deposition of the middle to upper parts of subtidal (MST-UST) zone . Detailed stratigraphic and facies analysis revealed that each cyclic sequence indicates a shallowing-upward deposition in a prograding carbonate platform (Shi et al. 2008; Tang et al. 2011). Accordingly, the studied MDSs appear in the upper unit of a meter-thick depositional cycle and were deposited in middle part of subtidal zone in a shallow carbonate platform (Tang et al., 2011).

Previously, these Wumishan MDSs were assigned to *Pseudogymnosolen* sp. (*sensu* Zhu et al., 1978; Liang et al., 1984; Cao, 1991; Qiu and Liang, 1993; Medvedev et al., 2005; Mei et al., 2008, 2010; Tang et al., 2013b). In contrast, other authors have treated similar MDSs from the Precambrian successions as a typical example of abiotic stromatolite (Grotzinger and Knoll, 1999; Grotzinger and James, 2000; Riding, 2008). Therefore, the specific scientific question for this work is “Are the Wumishan MDSs abiotic in origin?”

A zircon U–Pb age of 1622 ± 23 Ma is known from a tuff bed in the Dahongyu Formation in Jixian (Lu et al., 2008). Li et al. (2010) obtained zircon U–Pb dates of 1560 ± 5 Ma (LA-MC-ICP-MS) and 1559 ± 12 Ma (SHRIMP) from the same tuff bed at the upper Gaoyuzhuang Formation in Yanqing County, near Beijing. Li et al. (2014) dated a bentonite bed at the top of the Wumishan Formation and obtained zircon U–Pb ages of 1483 ± 13 Ma and 1487 ± 16 Ma. Su et al. (2010) reported zircon U-Pb ages of 1437 ± 21 Ma and 1372 ± 18 Ma from the overlying Tieling and Xiamaling formations of the Jixian Group, respectively (Fig. 1B). These zircon-based radiometric ages from the Mesoproterozoic succession in North China are thus all

self-consistent and contstrain the age of Wumishan Formation between 1483 ± 13 Ma and 1560 ± 5Ma.

3. Material and methods

Both polished slabs and petrologic thin sections were made to examine internal fabrics and diagenetic features of the stromatolite. Freshly broken and polished chips were prepared for thin sections and micro-analysis with an HITACHI-SU8010 Field Emission Scanning Electron Microscope (FESEM) equipped with an iXRF energy dispersive spectrometry (EDS). The samples were cleaned using DI water and coated with gold for surface texture imaging in secondary electron and EDS analysis. In this study, we employed Raman spectroscopy to assess the structural characteristics of organic matter in the stromatolites. A WITec α300 Confocal Raman system coupled with a Peltier-cooled EMCCD detector was used. Raman spectra were acquired using a 532 nm laser with output power between 3 to 10 mW, an aperture pinhole (optic fiber) of 50 μm in diameter, a 100 X objective, and an integration time of 0.5 seconds for 100 spectra that were averaged. Fluorescent imaging analysis is applied to check for the presence of organic matter in stromatolite using a Zeiss Scope.A1 fluorescence microscope X-Cite SERIES 120Q. Fluorescent images were captured under both blue exciting light (wavelength 450–490 nm) and purple exciting light (wavelength 510–560 nm). When these photons interact with organic matter in a specimen, a strong fluorescence is emitted in both green and red colours, respectively for the excitation wavelengths used. In contrast, when organic matter content is low, the rock appears dim and without fluorescence (Cuif et al., 1990; Reitner and Neuweiler, 1995; Russo et al., 1997, 2000; Mastandrea et al., 2006; Chen et al., 2014; Luo et al., 2016; Fang et al., 2017). The FESEM, micro-Raman, and fluorescence microscope are all locatedd at the State Key Laboratory of Biogeology and Environmental Geology (BGEG), China University of Geosciences, Wuhan. The terminology and methods to document stromatolite microfabrics follow Shapiro (2000) who observed microbial fabrics at three different scales.

4. Results

4.1. Non-stromatolite facies

Substrate of MDS comprises dolomitic limestone, which has a micritic texture (Fig. 3A). Microbial fossil fragments and cavity fills were usually recrystallized and altered to dolomite. Inter-columnar facies is dominated by micrite with abundant fragments of stromatolites and cavities filled with euhedral dolomite and siliceous crystallites. The capping facies of the MDS is dominantly composed of micrite occasionally with clotted structures, which have a typical thrombolitic texture (Fig. 3A, C).

4.2. Stromatolite macroscopic texture

In outcrops, diameter range of stromatolite columns stromatolites are 2-5 cm thick and occur as broad, laminated domes in the lower part of the section and digitate, low-relief columnar colonies in the upper part. Inter-columnar stromatolite spaces are filled with dolomite, micrite peloids, stromatolite fragments, and cavities (Figs. 3 and 4). Stromatolite columns are mostly 1-2 cm high and 0.2–0.8 cm wide, with maximum height up to 4.5 cm and width up to 1.0 cm. Low domical stromatolites initially developped on dolomitic wackestone (Fig. 3). In most cases, digitate, thin and low-relief columns developed on broad domal stromatolite (Fig. 3). The thin, digitate columns branch frequently (Figs. 3A and C), and occasionally merged together to form broad columnar colonies, which have second-order branching (Figs. 3A, and C). In plane view, discrete columns show small, concentrically laminar, circular to sub-circular domes, with densely packed and slightly convex or flat tops (Fig. 3B). These Wumishan stromatolites have patterns identical to those of other microdigitate stromatolites described from the Neoarchean to Paleoproterozoic (>1.6 Ga) (Schopf et al., 2007; Seong-Joo and Golubic, 1998, 1999; Shi et al., 2008; Kremer et al., 2012;

Wang et al., 2021).

On polished slabs, stromatolite columns comprise brown carbonate with distinct alternations of dark and light colored laminated layers in sharp contrast with interspaces between columns, which are typically composed of light colored dolomite and cavities with microspar (Fig. 3). The intercolumnar dolomite also shows authigenic columnar laminations (Fig. 3C). Crude laminae are flat to gently convex and crinkled (Figs 3A, 3C and 4A-C). Successive growth spheroids are evident in stromatolite columns (Figs. 3A and C). The laminae of a given growth stage are not necessarily parallel or convergent with the underlying laminae, but usually form gently convex laminar pattern in digitate columns and slightly wavy, the columnar branching and non-branching stromatolites with some turbinate (widening-upwards) and anastomosed (a window between conjoined columns that split and re-attach) structures (Figs. 3A and C).

4.3. Stromatolite microstructures visualized by microscopy

Under polarized light microscopy, light colored laminated layers are 30 to 160 μm in thickness (average around 60 μm), and often contain abundant, densely-packed light to dark brown spheroids. There are also abundant micron size dolomitic rhombs and some dolomite-filled cavities that appear clear and transparent (Fig. 4). In comparison, dark colored laminae are richer in organic matter and relatively thicker, between 200 and 1200 μm in thickness (average around 700 μm), and they are also filled with abundant small, rounded spheroids (Figs. 4E–G). Solitary spheroids often aggregated together to form consortia of clearer brown colour than the laminae in which they occur (Figs. 4E–G). Dark colored laminae are also occasionally disrupted by dolomite-filled cavities (Figs. 4C-E).

Most spheroids with single or double outlines, solitary or in small colonies are concentrated in dark colored laminae, with some scattered over entire MDS columns. Within spheroidal aggregates, a few solitary spheroids usually connect each other to form paired spheroids or short chains (Figs. 5, 6A and B). Single spheroids are mostly

15–30 μm in diameter with individuals having 20–25 μm diameters most frequently occurring (Fig. 5F).

Fibrous fabrics are also conspicuous under polarized light microscopy and are partly recrystallized and replaced by quartz (Fig. 5E, brown area). Single fibers are fine and between 10 and 15 μm in width, straight, and radially-oriented (Fig. 5E, white arrow). These vertically oriented fibers are more prominent in dark colored laminae than in light colored laminae. They usually penetrate laminae and some spheroids (Fig. 5E). In particular, many fibrous fabrics radiated to form individual spheroids with concentric laminations and their geometric centre is located where there are groups of spheroids.

Few transparent to translucent filaments composed of brown organic matter occur out of the columns (Figs. 6C and D). The filaments are about 5 μm in diameter, mostly straight or slightly curved and parallel-aligned, some are fractured, but none have branches. They are similar to the specimens reported in early discoveries (Liang et al., 1984).

Fluorescent imaging reveals that aggregates of spheroids have strong fluorescence under both green and purple exciting light. This contrasts with the absence or weak fluorescence of coarsely grained dolomite cement (Fig. 7). Strong fluorescence under both purple and green excitation indicates the presence of organic matter closely associated with the spheroids.

4.4. Nanoscopic structure (SEM observation)

4.4.1. Microscopic spheroids

SEM imaging shows high concentrations of tiny, rounded coccoid-like spheroids are pronounced in dark colored laminasets (Fig. 8). No framboidal aggregates of pyrite occur in the studied Wumishan stromatolites. However, two types of spheroids are distinguished. The first kind comprises micrite nuclei surrounded by sparitic sheaths, without nano-particle coatings (Figs 8). Like those observed under microscope, two or three solitary spheroids are usually connected to form pairs or

333 short chains, with the longest chain being composed of four or five spheroids (Figs.
334 8A–B, F–G). However, most spheroids occur as solitary individuals and they
335 aggregate to form consortia of dozens to hundreds of spheroids (Figs. 8A–B, F–G).
336 Single spheroids embrace nanoscopic grains on surfaces (Figs. 8C–D, 9B–H).
337 These nanoscopic grains are composed of tiny irregular sparitic calcite crystals that
338 are replaced by silica (Si, O elements) now (Fig. 8E). One distinct rounded opening
339 usually occurs on spheroid surface (Figs. 8 F-H, 9B, F–G, I). However, most openings
340 have irregular margins as outer envelopes are easily broken around the openings
341 possibly be due to diagenesis and silicification (Figs. 8F-H, 9H-I). The well-preserved
342 round openings are 3–8 μm in diameter and surrounded by 8–10 nano-crystals of
343 calcite that form rough and irregular edges (Fig. 9I). A few bacterial clump-like
344 nano-particle clusters are observed in nuclei when the outer envelope of some
345 spheroids is broken near the circular opening (Fig. 8G) or in cross section of single
346 spheroid (Fig. 9D).
347 The second kind of spheroids is usually enveloped with thin layers of
348 nanometer-scale particles (Figs. 10A–D). Most spheroids are fully coated with
349 nanoscopic grains (Figs. 10A, C–D), but some are only partly coated with
350 nano-particles (Fig. 10B) or, occasionally, lack outer nano-particle coatings (Fig. 9C).
351 When the coating nano-particles are removed, no circular openings are observed on
352 spheroid surface. Solitary spheroids comprise typically large nuclei of thick coarse
353 sparitic calcite crystal, 15–20 μm in diameter, coated with thin sparry sheaths, about 2
354 to 3 μm in thickness (Figs. 10C, F–G). The central crystal of spheroids is typically
355 replaced by silica (Figs. 10F–G) and represents an empty nucleus and indicating a
356 close empty system inside spheroid. EDS elemental mapping analysis shows that
357 single spheroids are, however, dominated by O, Si, Mg, Ca, and C that show
358 alternations between silicification of original carbonate and dolomitization (Fig. 10E).
359
360 *4.4.2. Nano-particles*
361 Carbonate nanometer-scale particles, comprising clusters of euhedral crystals
362 (Figs. 9G, I), are abundant and usually surround spheroid surfaces or scattered on

363 sediments (Figs. 10A–B, D). These nano-particles are mostly ellipsoidal or
364 subspheroidal to rhombus in outline, although some of them are amorphous (Figs. 9G,
365 I, 10B, F–G. Most nano-particles are 0.2–0.5 μm in diameter, with maximum size up
366 to 1 μm (Fig. 9I).

367 Some ultrastructures recognized by Tang et al. (2013a) from the Wumishan MDS
368 are also present in our samples, including filaments, films, nanoglobules (Ng), and
369 polyhedron (Po) aggregates (Figs. 11A–B, F–G). Polyhedra are extremely abundant
370 and 45–200 nm long. Small polyhedrons can coalesce into larger (100–200 nm)
371 polyhedrons (Fig. 8F), and also, together with nanoglobules, cluster to form
372 polyhedron aggregates (Fig. 11E). Nanoglobules are usually <45 nm in diameter.
373 They cluster to form polyhedron aggregates or other colonies (Figs. 11C–G).
374 Filaments and films are also seen to associate closely with all of these putative
375 organic components (Figs. 11F–G). They are partially replaced by small nanoglobules
376 or small polyhedrons (Figs. 11F–G). In addition, the dumbbell-shaped bursts of
377 nanoglobules are also well preserved and have two distinct bell-like aggregates (Figs.
378 11C–D), each 1.2–1.6 μm in diameter. They are connected by one short rod-like
379 structure, 1.0 to 1.2 μm long (Fig. 11C). The primitive form of dumbbell-shaped
380 bursts comprises two closely arranged bell-like aggregates, ~3.0 μm long (Fig. 11D).

381 EDS analysis indicates that polyhedrons (Fig. 11H), nanoglobules (Fig. 11I), and
382 mucuslike filaments (Fig. 11J) share the same elemental composition, all enriched in
383 Si and O, with subordinate amounts of C, Mg, and Ca, which indicates that calcified
384 organic relicts were replaced by silica during diagenetic silicification. In summary,
385 three types of nano-particles are evident in MDS laminae: (1) putative organic relics,
386 such as fragmented filaments and mucuslike biofilms (purported EPS), (2)
387 organominerals, including nanoglobules, polyhedrons, and their aggregates, and (3)
388 dumbbell-shaped microparticle aggregates.

389

390 *4.4.3. Raman spectroscopy of organic matter and associated minerals*

391 Laminated domal stromatolites with and without spheroids were analyzed by
392 micro-Raman spectroscopy (Figs. 12 and 13). Raman spectra show that the typical

features of disordered organic matter with the two main broad bands centered at around 1350 and 1600 cm^{-1} in the laminated dome without spheroids (Fig.12). Raman spectra of carbonate in the domal stromatolite have bands at 154, 281, 712 and 1086 cm^{-1} that are assigned to calcite (Fig. 12B). Raman spectra show the typical features of disordered organic matter with two broad bands at around 1350 and 1600 cm^{-1} in the rims of microscopic spheroids (Fig. 13B), which are identical to organic matter from domal stromatolites without spheroids (Fig. 12B). The organic matter in the spheroids also has a peak at 465 cm^{-1}, which represents microcrystalline quartz in their interior (Fig. 13). The bands at 176 and 299 cm^{-1}, and most notably at 1090 cm^{-1} for the main carbonate peak, occur in the Raman spectra of organic matter in the host rock, indicating the occurrence of dolomite in the mineral matrix (Rividi et al., 2010).

In this study, we use the intensity ratio of the band at 1350 vs.1600 cm^{-1} (denoted as I-1350/1600, Figs. 12 and 13), to characterize the structural order of organic matter (Bonal et al., 2006; Foucher et al., 2015; Qu et al., 2015, 2017, 2018). In order to further investigate this organic matter and associated minerals, two-dimensional Raman hyperspectral imaging was performed (Figs. 12 and 13). The intensities of the bands at 1350 cm^{-1} and 1600 cm^{-1} confirms the ubiquitous presence of organic matter in the MDS. The Raman spectral parameter I-1350/1600 reflects changes in the degree of disorder of the organic matter. The D-band and G-band maps show high concentrations of organic carbon in discontinuous organic laminae and spheroids in the stromatolites (Figs. 12B and 13B).

5. Discussion

5.1. Morphology of the Wumishan MDS

Both macroscopic and microscopic features of the Wumishan stromatolites are identical to that of typical microdigitate stromatolites, which have been described from the Neoarchean to Paleoproterozoic (>1.6 Ga) worldwide (Grotzinger and Reed, 1983; Hofmann and Jackson, 1987; Knoll et al., 1993; Sergeev et al., 1995;

423 Grotzinger and Knoll, 1999; Tang et al., 2013b). In North China, the morphologically
424 identical tiny stromatolites were first reported by Liang et al (1984) from the
425 Wumishan Formation of the Jixian section, Tianjin City, North China. Similar forms
426 of stromatolites were later discovered in many other places, such as Eastern Asia,
427 North America, Australia, and South Africa (Liang et al., 1984; Grey, 1984; Grey and
428 Thorne, 1985; Hofmann and Jackson, 1987). These MDSs have been assigned to
429 different taxa, such as *Microstylus* in Siberia (Komar et al., 1966), *Asperia* in Canada
430 (Semikhatov et al., 1979), *Lenia-Stratifera* in Hudsun Bay, South Africa (Hofmann,
431 1977), and *Pseudogymnosolen* in China (Liang et al., 1984). They, however, should
432 belong to the same taxon in terms of similar shape, size, type of branches, structure of
433 sidepiece, and microfabrics (Liang et al., 1984). In Jixian some putative filamentous
434 cyanobacteria were also found in the cherts in which the stromatolites grew (Liang et
435 al., 1984), and most of them are identical to *Eomycetopsis* Schopf. However, none of
436 them occurred in stromatolite columns or laminae, but in the interspace between
437 columns and inter-stromatolite parts (Liang et al., 1984). Accordingly, the possible
438 stromatolite-builders have long remained enigmatic.
439
440 *5.2. Geobiologic features and biosignatures*
441
442 *5.2.1. Filaments and spheroids*
443 Liang et al. (1984) identified these filaments as *Eomycetopsis* Schopf (1968),
444 *Animikiea* Barghoorn (1965) and *Rhicnonema* Hofmann (1976) based on their
445 colonial characteristics and morphology. Here, the filaments can be identified as
446 *Siphonophycus* sp., most similar to reported occurrences from the Bitter Spring
447 Formation in Australia. Their characteristic elongated morphology of transparent to
448 translucent body bound by organic cell walls, and without branches and separation
449 which were different from the *Eomycetopsis* sp., *Aninikiea* sp., and *Rhicnonema* sp.
450 Although some Archean–Paleoproterozoic spheroids are suspected to be
451 pseudofossils (Rouillard et al., 2020), many similar coccoid-like spheroids have been
452 widely reported in microbial mat deposits and stromatolites from both ancient and

453 modern environments (Folk, 1993; Reid et al., 2000; Kremer and Kazmierczak, 2005;
454 Perri and Tucker, 2007; Brigmon et al., 2008; Noffke and Awramik, 2013; Chen et al.,
455 2014; Luo et al., 2014; Lan et al., 2020). These spheroidal objects are usually
456 interpreted as either fossilized bacteria (Folk, 1993; Reid et al., 2000; Noffke et al.,
457 2003; Chen et al., 2014; Luo et al., 2014, 2016; Fang et al., 2017; Wu et al., 2017) or
458 mineral forms induced abiotically or biologically (Brigmon et al., 2008). The
459 Wumishan spheroids resemble coccoid-like objects in most observed aspects,
460 however they are about two times larger than the coccoid-like spheroids reported
461 elsewhere (She et al., 2014). In particular, fluorescent imaging reveals that spheroidal
462 aggregates also tend to form consortium (Fig. 7), which resembles remarkably unicell
463 colonies of the cyanophytic affinity in present-day stromatolites (Schopf and Sovietov,
464 1976). In addition, strong fluorescence under both purple and green excitation
465 indicates the presence of organic matter, as observed in stromatolites of other ages
466 (Cuif et al., 1990; Reitner and Neuweiler, 1995; Russo et al., 1997, 2000; Mastandrea
467 et al., 2006; Chen et al., 2014). Lastly, while there exists a range of abiotic biomorphs
468 that can form spheres similar spherical morphology and siliceous composition as
469 those observed in the Wumishan MDS (Rouillard et al., 2018; García-Ruiz, 1994), the
470 geobiological context of the Wumishan stromatolite specimens, co-occurrence with
471 filamentous micro-structures, and abundance of organic matter makes it more likely
472 that the Wumishan spheroids are biological in origin. Hence, the Wumishan spheroids
473 likely represent fossilized bacteria, which may have built the Wumishan MDSs or
474 contributed to biomineralization as they are common in laminae.

475 Zhang (1985) described a diverse microbiota from the Wumishan MDS of the
476 adjacent Beijing area. Of these, cell-like coccoids assigned to *Myxococcoides* sp.,
477 resemble superficially spheroids documented here in morphology and size. The
478 former are abundant and densely packed. They constitute the main part of the
479 organic-rich laminae and have been considered as the main mat-builders (Zhang,
480 1985). Similarly, the colonized coccoid-like spheroids are abundant and form dense
481 populations in the Wumishan MDS. The Wumishan spheroids therefore may also
482 have played a similar role in building the MDS, like those cell-like coccoids reported

from the same formation of the Beijing area (Zhang, 1985).

The distinct rounded openings are commonly observed on spheroidal surfaces in the Wumishan MDS (Figs. 8H-J, 9F-I). Bacterial clump-like particles occasionally aggregated to cluster in the nuclei of spheroids (Fig. 8J). Similar circular openings are also commonly present on these coccoid-like spheroids reported from the Mesoproterozoic Gaoyuzhuang and Wumishan formations of the adjacent Beijing and Hebei areas, North China (Zhang, 1981, 1985). This peculiar structure has been interpreted as division point of unicells during reproduction of the life cycle of unicellular microorganisms. The cell divided from this circular opening into two, three, and four, up to more within an envelope, and the parental envelope released the enclosed daughter cells (Zhang, 1981), which is an interpretation previously invoked for the life cycle of some Precambrian microfossils (Knoll and Barghoorn, 1977; Knoll and Golubic, 1979). Although the reproduction series of a complete life cycle of prokaryotes is not observed in the Jixian materials, co-existence of microscopic bacterial clusters and relatively large spheroids with thin envelopes indicate these cell-like spheroids may have experienced similar reproduction style as part of their life cycle.

Zhao et al. (2020) reported abundant coccoids from the microbial mats recorded in the third member of the Wumishan Formation of the Jixian Group. These coccoids are distributed along the beddings and were identified as *Myxococcoides* sp., which have also been recognized from the Wumishan Formation in the Jixian area (Wang et al., 2021). These microfossils are simple in morphology and uniform in size, and show various degrees of degradation. They are almost identical to the newly obtained spheroids from the Wumishan MDS in this study. In addition, comparable coccoid-like spheroids have been widely reported from the Archean to Paleoproterozoic successions worldwide, for instance, colonial ensheathed coccoidal unicells from the ca 3388 Myr old Strelley Pool Chert of Western Australia (Schopf and Packer, 1987; Schopf, 1992), and solitary or paired microbial coccoidal unicells and bacterium-like rod-shaped unicells from the ~3260 Ma Swartkoppie Formation and the ~2600 Ma Monte Cristo Formation of South Africa (Lanier, 1986; Buick,

2001). All of these Archean–Paleoproterozoic solitary or paired coccoid-like spheroids have been interpreted as a biogenic origin because they are composed of organic matter, and special microstructure with biological characteristics.

5.2.2. Nano-particles

Tang et al. (2013a) documented three kinds of ultrastructures from the dark laminasets of the MDS columns: (1) putative organic relics, such as filaments, their fragments, and mucuslike films or filaments (purported extracellular polymeric substances (EPS), (2) organo-minerals, including nanoglobules, polyhedrons, and their aggregated microparticles, and (3) euhedral crystals mainly constituting microsparitic strips and the rims surrounding microparticles. The first two types of nano-particles are also common in the Jixian samples. Filaments, relics of putative EPS, microparticles, and nanoglobules have been interpreted as organo-mineralized features, suggestive of a biogenic origin for the Wumishan MDS (Tang et al., 2013b).

It is also known that EPS plays a crucial role not only in calcium carbonate precipitation (Riding, 2000; Dupraz et al., 2004, Dupraz and Visscher, 2005; Braissant et al., 2007; Bontognali et al., 2010; Chen et al., 2014; Luo et al., 2014; Chen et al., 2019), but also in dolomitization processes under subsurface condition (Bontognali et al., 2010; Krause et al., 2012). This is because EPS might have served as a template to induce the dolomite formation directly from solutions, and exopolymeric substances were visualized as an alveolar organic network, within which precipitation of dolomite was initiated (Bontognali et al., 2010). The ability of EPS to preferentially bind Mg and Si over Ca may play a crucial role in overcoming the kinetic barriers that prevent nucleation of dolomite in subsurface environments (Bontognali et al., 2010).

Silicified virus-like nanoparticles have been interpreted to occur in biofilms that grow around modern hot spring (Peng et al., 2013). Their microstructure is similar to the nanoscopic grains documented here on the surface of spheroids. Pacton et al (2014) used contextual metagenomic data and microscopic analyses to show that viruses occur in high diversity within a modern lacustrine microbial mat, and vastly outnumber prokaryotes and other components of the microbial mat. Hence, the

543 nano-particles such as polyhedra and nano-globules found in the MDSs and in
544 association with spheroidal microfossils may be silicified bacteriophage-types of
545 viruses. It should be noted that many of these nano-particles were described from
546 radial-fibrous textures in the Wumishan MDS. Similar nano-particles have also been
547 found in association with abundant rod-like aggregates from radial fibrous fabrics in
548 cement fans of small noduar microbialites from the Permian-Triassic boundary beds
549 in the Tieshikou section of Jiangxi Province, South China (Yang et al., 2019). In the
550 Permian-Triassic samples, the he irregular nanoparticles, but mostly fibrous biofilms
551 frequently are seen in the dolomite crystals when their surfaces are corroded (Yang et
552 al., 2019). Similar fibrous biofilms have also been reported from
553 dolomite-precipiating environment of a Miocene lacustrine system (Sanz-Montero et
554 al., 2008) and are also commonly present in modern and fossilized stromatolites and
555 microbial mats, and they have been interpreted as EPS remains (Dupraz and Visscher,
556 2005; Noffke, 2010; Luo et al., 2013, 2014; Tu et al., 2016; Xu et al., 2017; Decho
557 and Gutierrez, 2017; Yang et al., 2017). Accordingly, the radial fibrous fabrics from
558 the Mesoproterozoic to Phanerozoic and modern stromatolites and microbial mats are
559 likely of biogenic origin and some heterotrophic bacteria may have involved in
560 facilitating the precipitation of radial fibers in camodern and deep-time rbonate
561 precipitates. However, whether these nano-particles obtained from geological samples
562 can be compared directly to modern EPS remains to be determined (Dupraz et al.,
563 2009; Decho and Gutierrez, 2017). This is because few studies have revealed how
564 diagenesis affects the lithification of EPS from living objects to fossilized forms. Thus,
565 this interpretation, rests on comparisons of morphology and size dimensions and
566 therefore, more work is needed to determine the true origin of these nano-particles.

567 Besides, both–clump-shaped and dumbbell-shaped nanoglobule aggregates are
568 common in the silicified laminae of the Wumishan MDSs (Figs. 11C–E). Some
569 nano-particles still have relicts of minute dolomite rhombs, although they were mostly
570 replaced by silica due to silicification. The dumbbell-shaped aggregates of
571 nano-particles are usually considered an indication of microbial formation of dolomite
572 in modern and ancient environments (Vasconcelos et al., 1995; Vasconcelos and

573 Mckenzie, 1997; García Delcura et al., 2001), strengthening the interpretation that the
574 nano-particles of MDS are biogenic in origin (Tang et al., 2013b). However,
575 microscopic dumbbell-shaped mineral habits have also been produced abiotically in
576 laboratory diagenetic experiments with apatite (Blake et al., 1998). Their exceptional
577 preservation is probably, in part, due to early silicification that is critical for the
578 preservation of microfabrics and organominerals in the MDSs (Tang et al., 2013b).
579 The amorphous silica surrounding microscopic spheroids (Fig. 9G) indicates that the
580 silicon replacement was earlier than complete degradation of organic matrix or EPS
581 (Bartley et al., 2000; Berelson et al., 2011). Hence, the combination of evidence from
582 the MDSs of the middle Mesoproterozoic Wumishan Formation is consistent with a
583 biogenic origin for this type of stromatolites.
584
585 **6. Conclusions**
586
587 The Wumishan stromatolites are identical to the microdigitate stromatolites in the
588 Neoarchean to Paleoproterozoic (>1.6 Ga) oceans. The dark colored laminasets
589 contain abundant and densely-packed coccoid-like spheroids, mostly 15–30 μm in
590 diameter, which have single or double outlines, and occur as solitary individuals but
591 most often in small colonies akin to *Myxococcoides*. Strong fluorescence under both
592 green and purple exciting light indicates that their composition is dominated by
593 organic matter, which is independently confirmed by Raman hyperspectral imaging of
594 highly disordered, indigenous organic matter. Vertically to radially oriented fibrous
595 fabrics, often with equidistant, circularly concentric layers of organic matters are
596 pronounced and usually penetrate laminae and some spheroids, suggesting abiotic
597 genesis for these mineralised growth features. The circular concentricity of patterns in
598 the MDSs also displays gradients of variable density of organic matter and are also
599 formed by radially aligned quartz crystals, all of which are geometric patterns
600 displayed also by chemically oscillating reactions during the oxidation of malonic
601 acid by bromate and sulfuric acid to carbon dioxide. Microscopic spheroids in the
602 Wumishan MDSs have two morphologies. The first kind comprises micrite nuclei

surrounded by sparitic sheaths, without nano-particle coatings, but with one distinct micron-size rounded opening. The nuclei are usually filled with clump-like nano-particles. The second kind of spheroids is enveloped with thin layers of nano-particles, lacks a circular opening on its surface, and possesses large nuclei of single-crystal coarse sparitic calcite coated with thin sparry sheaths, representing an empty nucleus. These coccoid-like spheroids resemble cell-like coccoids reported from the Archean-Paleoproterozoic rocks worldwide. Both rounded openings on spheroid surfaces and microbial clump-like nano-particle aggregates in microscopic spheroids may represent the reproduction process (cell-division) part of the life cycle of micro-organisms. This could have occurred if the cells divided from the rounded openings into two or more cells within the same envelope, followed by the parental envelope releasing more daughter cells, in line with interpretations of other coccoidal microfossils reported from elsewhere. The Wumishan microscopic spheroids therefore represent fossilized microbes that likely contributed to construct the MDSs. Three types of nano-particles were found to occur: (1) putative organic relics, such as mucuslike biofilms (purportedly EPS), (2) organominerals including nanoglobules, polyhedrons, and their aggregates, and (3) dumbbell-shaped nano-particle aggregates are also of possible biogenic origin. The multiple different types of biosignatures reported in the Wumishan MDS thus allow greater confidence in assigning a biogenic origin to these notable and enigmatic radial-fibrous fabrics and stromatolite morphologies.

Acknowledgements

We are grateful to guest editor Zhongwu Lan, and both reviewers Yi-Ni Wang and Dongjie Tang for their critical comments and constructive suggestions that have improved greatly the quality of the paper. This study was supported by a National Key R & D Program of China grant (2017YFC0603103), a NSFC grant (41821001), and the 111 Program of China (BP0820004).

References

Allwood, A.C., Walter, M.R., Kamber, B.S., Marshall, C.P., Burch, I.W., 2006. Stromatolite reef from the early Archaean era of Australia. Nature 441, 714–718.

Altermann, W., Kazmierczak, J., Oren, A., Wright, D.T., 2006. Cyanobacterial calcification and its rock-building potential during 3.5 billion years of Earth history. Geobiology 4, 147–166.

Awramik, S.M., 1971. Precambrian columnar stromatolite diversity: reflection of metazoan appearance. Science 174, 825–827.

Awramik, S.M., 2006. Respect for stromatolites. Nature 441, 700-701.

Awramik, S.M., Margulis, L., 1974, Definition of stromatolite. In: Walter, E. (Ed.), Stromatolite Newsletter 2, p. 5.

Awramik, S.M., Sprinkle, J., 1999. Proterozoic stromatolites: the first marine evolutionary biota. Historical Biology 13, 24–253.

Bartley, J.K., Knoll, A.H., Grotzinger, J.P., Sergeev, V.N., 2000. Lithification and fabric genesis in precipitated stromatolites and associated peritidal carbonates, Mesoproterozoic Billyakh Group, Siberia. In: Grotzinger, J.P., James, N.P. (eds), Precambrian Carbonates. Society for Sedimentary Geology (SEPM), Special Publication 65. Tulsa, Oklahoma, pp. 59–74.

Baumgartner, R.J., Van Kranendonk, M.J., Fiorentini, M.L., Pages, A., Wacey, D., Kong, C., Saunders, M., Ryan, C., 2020. Formation of micro-spherulitic barite in association with organic matter within sulfidized stromatolites of the 3.48 billion-year-old Dresser Formation, Pilbara Craton. Geobiology 18, 415–425.

Berelson, W.M., Corsetti, F.A., Pepe-Ranney, C., Hammond, D.E., Beaumont, W., Spear, J.R., 2011. Hot spring siliceous stromatolites from Yellowstone National Park: Assessing growth rate and laminae formation. Geobiology 9, 411–424.

Blake, R.E., O'Neil, J.R., Garcia, G.A. 1998. Effects of microbial activity on the delta ^{18}O of dissolved inorganic phosphate and textural features of synthetic apatites. American Mineralogist 83, 1516–1531.

Bonal, L., Quirico, E., Bourot-Denise, M., Montagnac, G., 2006. Determination of the petrologic type of CV3 chondrites by Raman spectroscopy of included organic matter. Geochimica Cosmochimica Acta 70, 1849–1863.

Bontognali, T.R., Vasconcelos, C., Warthmann, R.J., Bernasconi, S.M., Dupraz, C., Strohmenger, C.J., Mckenzie, J.A., 2010. Dolomite formation within microbial mats in the coastal sabkha of Abu Dhabi (United Arab Emirates). Sedimentology 57, 824–844.

Braissant, O., Decho, A.W., Dupraz, C., Glunk, C., Przekop, K.M., Visscher, P.T., 2007. Expolymeric substances of sulfate-reducing bacteria: interactions with calcium at alkaline pH and implication for formation of carbonate minerals. Geobiology 5, 401–411.

Brigmon, R., Morris, P., Smith, G., 2008. Evaporite microbial films, mats, microbialites and stromatolites. In: Dilek, Y., Furnes, H., Muehlenbachs, K. (eds), Links between Geological Process, Microbial Activities and Evolution of Life. Springer, pp. 197–235.

Buick, R., 2001. Life in the Archean. In: Briggs, D.E.G., Crowther, P.R. (eds), Paleobiology II. Blackwell Science, Oxford, London, pp. 13–21.

Cao, R., 1991. Origin and order of cyclic growth patterns in mat-ministromatolite bioherms from the Proterozoic Wumishan Formation, North China. Precambrian Research 52, 167–178.

Chen, J., Zhang, H., Zhu, S., Zhao, Z., Wang, Z., 1980. Research on Sinian Suberathem of Jixian. In: Tianjin Institute of Geology and Mineral Resources (Ed.), Sinian Suberathem in China. Tianjin Science and Technology Press, Tianjin, pp. 56–114.

Chen, Z.Q., Wang, Y.B., Kershaw, S., Luo. M., Yang, H., Zhao, L.S., Fang, Y.H., Chen, J.B., Li, Y., Zhang, L., 2014. Early Triassic stromatolites in a siliciclastic nearshore setting in northern Perth Basin, Western Australia: geobiologic features and implications for post-extinction microbial proliferation. Global and Planetary Change 121, 89–100.

Cuif, J.P., Gautret, P., Laghi, G.F., Mastandrea, A., Pradier, B., Russo, F., 1990. Recherche sur la fluorescence UV du squelette aspiculaire chez les demosponges calcitiques triasiques. Geobios 23, 21–31.

Decho, A.W., Gutierrez, T., 2017. Microbial extracellular polymeric substances (EPSs) in ocean systems. Frontier in Microbiology 8, 922e.

Dupraz, C., Visscher, P.T., 2005. Microbial lithification in marine stromatolites and hypersaline mats. Trends in Microbiology 13, 429-439.

Dupraz, C., Visscher, P.T., Baumgartner, L.K., Reid, R.P., 2004. Microbe-mineral interactions: early carbonate precipitation in a hydpersaline lake (Eleuthera Island, Bahamas). Sedimentology 51, 745–765.

Dupraz, C., Reid, R.P., Braissant, O., Decho, A.W., Norman, R.S., Visscher, P.T., 2009. Process of carbonate precipitation in modern microbial mats. Earth-Science Reviews 96, 41–162.

Fang, Y.H., Chen, Z.Q., Kershaw, S., Li, Y., Luo, M., 2017. An Early Triassic (Smithian) stromatolite associated with giant ooid banks from Lichuan (Hubei Province), South China: Environment and controls on its formation. Palaeogeography, Palaeoclimatology, Palaeoecology 486, 108–122.

Foucher, F., Ammar, M.R., Westall, F., 2015. Revealing the biotic origin of silicified Precambrian carbonaceous microstructures using Raman spectroscopic mapping, a potential method for the detection of microfossils on Mars. Journal of Raman Spectroscope 46, 873–879.

Folk, R.L., 1993, SEM Imaging of bacteria and nannobacteria in carbonate sediments and rocks. Journal of Sedimentary Petrology 63, 990–999.

Fralick, P., Riding, R., 2015. Steep Rock Lake: Sedimentology and geochemistry of an Archean carbonate platform. Earth-Science Reviews 151, 132–175.

García-Ruiz, J.M. 1994. Inorganic self-organisation in precambrian cherts. Origins of Life and Evolution of Biospheres 24, 451–467.

García Delcura, M.A., Salvador Ordóñez, J.C., Jones, B.F., Cañaveras, J.C., 2001. Petrology and geochemical evidence for the formation of primary bacterially induced lacustrine dolomite: La Roda ‘white earth’ (Pliocene, central Spain). Sedimentology 48, 897–915.

723 Glunk, C., Dupraz, C., Braissant, O., Gallagher, K.L., Verrecchia, E.P., Visscher, P.T.,
724 2011. Microbially mediated carbonate precipitation in a hypersaline lake, Big
725 Pond (Eleuthera, Bahamas). Sedimentology 58, 720–736.
726 Goodwin, A., Papineau, D. 2021. Biosignatures Associated with Organic Matter in
727 Late Paleoproterozoic Stromatolitic Dolomite and Implications for Martian
728 Carbonates. Astrobiology, in press, http://doi.org/10.1089/ast.2021.0010
729 Grey, K., 1982. Aspects of Proterozoic stromatolite biostratigraphy in Western
730 Australia. Precambrian Research 29, 347–365.
731 Grey, K., Thorne, A.M., 1985. Biostratigraphic significance of stromatolites in
732 upward shallowing sequences of the early Proterozoic Duck Creek dolomite,
733 Western Australia. Precambrian Research 29, 183–206.
734 Grotzinger, J.P., James, N.P., 2000. Precambrian carbonates: evolution of
735 understanding. In: Grotzinger, J.P., James, N.P. (eds), Carbonate Sedimentation
736 and Diagenesis in the Evolving Precambrian World. Society for Sedimentary
737 Geology (SEPM), Special Publication 67, Tulsa, Oklahoma, pp. 3–20.
738 Grotzinger, J.P., Knoll, A.H., 1999. Stromatolites in Precambrian carbonates:
739 evolutionary mileposts or environmental dipsticks? Annual Review of Earth and
740 Planetary Sciences 27, 313–358.
741 Grotzinger, J.P., Reed, J.F., 1983. Evidence for primary aragonite precipitation, lower
742 Proterozoic (1.9 Ga) dolomite, Wopmay orogen, northwest Canada. Geology 11,
743 710–713.
744 Hofmann, H.J., 1977. The problematic fossil *Chuaria* from the Late Precambrian
745 Uinta Mountain Group, Utah. Precambrian Research 4, l–ll.
746 Hofmann, H.J., 2000. Archean stromatolites as microbial archives. In: Riding, R.,
747 Awramik, S.M. (eds), Microbial Sediments. Springer-Verlag, Berlin, Heidelberg,
748 pp. 315–327.
749 Hofmann, H.J., Jackson, G.D., 1987. Proterozoic ministromatolites with radial-fibrous
750 fabric. Sedimentology 34, 963–971.
751 Horodyski, R.J., Donaldson, J.A., 1980. Microfossils from the Middle Proterozoic
752 Dismal Lakes Group, Arctic Canada. Precambrian Research 11, 125-159.
753 James, N.P., Narbonne, G.M., Sherman, A.G., 1998. MT carbonates: shallow subtidal
754 facies of the mid to late Proterozoic. Journal of Sedimentary Research 68,
755 716–722.
756 Kah, L.C., Riding, R., 2007. Mesoproterozoic carbon dioxide levels inferred from
757 calcified cyanobacteria. Geology 35, 799–802.
758 Knoll, A.H., 2013. Systems paleobiology. Geological Society of America Bulletin
759 125, 3–13.
760 Knoll, A.H., Barghoorn, E.S., 1977. Archean microfossils showing cell division from
761 the Swaziland System of South Africa. Science 198, 396–398.
762 Knoll, A.H., Golubic, S., 1979. Anatomy and taphonomy of a Precambrian algal
763 stromatolite. Precambrian Research 10, 115–151.
764 Knoll, A.H., Semikhatov, M.A., 1998. The genesis and time distribution of two
765 distinctive Proterozoic stromatolitic microstructures. Palaios 13, 407–421.

766 Knoll, A.H., Grotzinger, J.P., Sergeev, V., 1993. Carbonate precipitation in stratiform
767 and domal structures from the Mesoproterozoic Kotuikan Formation, northern
768 Siberia. Geological Society of America, Abstracts with Programs 25, p. 357.
769 Komar, V.A., 1966. Upper Precambrian stromatolites of the northern part of the
770 Siberian Platform and their stratigraphic significance. Transactions of the
771 Geological Institute, 154, Nauka, Moscow (1966), 122 pp. (in Russian).
772 Kremer, B., Kazmierczak, J. 2005. Cyanobacterial mats from Silurian black
773 radiolarian cherts: phototrophic life at the edge of darkness? Journal of
774 Sedimentary Research 75, 897–906.
775 Kremer, B., Kazmierczak, J., Łukomska-Kowalczyk, M., Kempe, S., 2012.
776 Calcification and silicification: fossilization potential of cyanobacteria from
777 stromatolites of Niuafos Caldera Lakes (Tonga) and implications for the early
778 fossil record. Astrobiology 12, 535–548.
779 Krause, S., Liebetrau, V., Gorb, S., Sánchez-Román, M., Mckenzie, J., Treude, T.,
780 2012. Microbial nucleation of Mg-rich dolomite in exopolymeric substances
781 under anoxic modern seawater salinity: new insight into an old enigma. Geology
782 40, 587–590.
783 Lan, Z.W., Zhang, S.J., Tucker, M., Li, Z.S., Zhao, Z.Y., 2020. Evidence for microbes
784 in early Neoproterozoic stromatolites. Sedimentary Geology 398, 105589.
785 Lanier, W.P., 1986. Approximate growth rates of Early Proterozoic
786 microstromatolites as deduced by biomass productivity. Palaios 1, 525–542.
787 Li, H., Shu, W., Zhou, H., Xiang, Z., Tian, H., Yang, L., Huff, W.D., Ettensohn, F.R.,
788 2014. The first precise age constraints on the Jixian System of the Meso-to
789 Neoproterozoic standard section of China: SHRIMP zircon U-Pb dating of
790 bentonites from the Wumishan and Tieling formations in the Jixian section, North
791 China Craton. Acta Petrologica Sinica 30, 2999–3012.
792 Li, H.K., Zhu, S.X., Xiang, Z.Q., Su, W.B., Lu, S.N., Zhou, H.Y., Geng, J.Z., Li, S.,
793 Yang, F.J., 2010. Zircon U-Pb dating on tuff bed from Gaoyuzhuang Formation
794 in Yanqing, Beijing: further constraints on the new subdivision of the
795 Mesoproterozoic stratigraphy in the northern North China Craton. Acta
796 Petrologica Sinica 26, 2131–2140.
797 Liang, Y.Z., Cao, R.J., Zhang, Y.L., 1984. On the Precambrian
798 *Pseudogymnosolenaceae* Stromatolites. Geological Publishing House, Beijing,
799 199 pp.
800 Lu, S.N., Zhao, G.C., Wang, H.C., Hao, G.J., 2008. Precambrian metamorphic
801 basement and sedimentary cover of the North China Craton: a review.
802 Precambrian Research 160, 77–93.
803 Luo, M., Chen, Z.Q., Hu, S.X., Zhang, Q.Y., Benton, M.J., Zhou, C.Y., Wen, W.,
804 Huang, J.Y., 2013. Carbonate reticulated ridge structures from the lower Middle
805 Triassic of the Luoping area, Yunnan, southwestern China: geobiological features
806 and implications for exceptional preservation of the Luoping biota. Palaios 28,
807 541–551.
808 Luo, M., Chen, Z.Q., Zhao, L.S., Kershaw, S., Huang, J.Y., Wu, L.L., Yang, H., Fang,
809 Y.H., Huang, Y.G., Zhang, Q.Y., Hu, S.X., Zhou, C.Y., Wen, W., Jia, Z.H., 2014.

Early Middle Triassic stromatolites from the Luoping area, Yunnan Province, Southwest China: Geologic features and environmental implications. Palaeogeography, Palaeoclimatology, Palaeoecology 412, 124–140.

Luo, M., Chen, Z.Q., Shi, G. R., Fang, Y.H., Song, H.J., Jia, Z.H., Huang, Y.G., Yang, H., 2016. Upper Lower Triassic stromatolite from Anhui, South China: Geobiologic features and paleoenvironmental implications. Palaeogeography, Palaeoclimatology, Palaeoecology 452, 40–54.

Mastandrea, A., Perri, E., Russo, F., Spadafora, A., Tucker, M., 2006. Microbial primary dolomite from a Norian carbonate platform: northern Calabria, southern Italy. Sedimentology 53, 465–480.

Medvedev, P., Bekker, A., Karhu, J.A., Kortelainen, N., 2005. Testing the biostratigraphic potential of early Paleoproterozoic microdigitate stromatolites. Revista Espanõla de Micropaleontología 37, 41–56.

Mei, M.X., Ma, Y.S., Guo, Q.Y., 2001. Basic litho-faces-succession model for Wumishan cyclothems: Their Markov chain analysis and regularly vertical stacking pattern in the third-order sequences. Acta Geologica Sinica, English Edition 75, 421–431.

Mei, M.X., Gao, J.H., Meng, Q.F., Liu, Z.R., 2008. Microdigital stromatolites and their response to stromatolite decline at 1250 Ma ± for the Mesoproterozoic Wumishan Formation at Jixian section in Tianjin. Journal of Palaeogeography 10, 495–509.

Mei, M.X., Gao, J.H., Meng, Q.F., Liu, Z.R., 2010. Sedimentary features and their implications of microdigital stromatolites from the Mesoproterozoic Wumishan Formation at Jixian Section in North China. Acta Geologica Sinica (English Edition) 84, 483–496.

Noffke, N., 2010. Geobiology: Microbial Mats in Sandy Deposits From the Archean Era to Today. Springer (193 pp).

Noffke, N., Awramik, S.M., 2013. Stromatolites and MISS–differences between relatives. GSA Today 23, 4–9.Noffke, N., Gerdes, G., Klenke, T., 2003. Benthic cyanobacteria and their influence on the sedimentary dynamics of peritidal depositional systems (siliciclastic, evaporitic salty, and evaporitic carbonatic). EarthScience Reviews 62, 163–176.

Nutman, A., Bennett, V., Friend, C., van Kranendonk, M.J., Chivas, A.R., 2016. Rapid emergence of life shown by discovery of 3,700-million-year-old microbial structures. Nature 537, 535–538.

Pacton, M., Wacey, D., Corinaldesi, C., Tangherlini, M., Kilburn, M.R., Gorin, G.E., Danovaro, R., Vasconcelos, C. 2014. Viruses as new agents of organomineralization in the geological record. Nature Communications 5, 4298e.

Papineau, D., 2020. Chemically oscillating reactions in the formation of botryoidal malachite. American Mineralogist 105, 447–454.

Peng, X., Xu, H., Jones, B., Chen, S., Zhou H., 2013. Silicified virus-like nanoparticles in an extreme thermal environment: implications for the preservation of viruses in the geological record. Geobiology 11, 511–526.

Perri, E., Tucker, M., 2007. Bacterial fossils and microbial dolomite in Triassic stromatolites. Geology 35, 207–210.
Qiu, S.Y., Liang, Y.Z., 1993. A restudy of *Pseudogymnosolenaceae*. Acta Palaeontologica Sinica 32, 123–128.
Qu, Y., Engdahl, A., Zhu, S., Vajda, V., McLoughlin, N., 2015. Ultrastructural heterogeneity of carbonaceous material in ancient cherts: investigating biosignature origin and preservation. Astrobiology 15, 825–842.
Qu, Y., Wang, J., Xiao, S., Whitehouse, M., Engdahl, A., Wang, G., McLoughlin, N., 2017. Carbonaceous biosignatures of diverse chemotrophic microbial communities from chert nodules of the Ediacaran Doushantuo Formation. Precambrian Research 290, 184–196.
Qu, Y., Zhu, S., Whitehouse, M., Engdahl, A., McLoughlin, N., 2018. Carbonaceous biosignatures of the earliest putative macroscopic multicellular eukaryotes from 1630 Ma Tuanshanzi Formation, north China. Precambrian Research 304, 99–109.
Reitner, J., Neuweiler, F., 1995. Mud mounds: a polygenic spectrum of fine-grained carbonate buildups. Facies 32, 1–70.
Reid, R.P., Visscher, P.T., Decho, A.W., Stolz, J.F., Bebout, B.M., Dupraz, C., MacIntyre, I.G., Paerl, H.W., Pinckney, J.L., Prufert-Bebout, L., Steppe, T.F., DesMarais, D.J., 2000. The role of microbes in accretion, lamination, and early lithification of modern marine stromatolites. Nature 406, 989–992.
Riding, R., 2000. Microbial carbonates: the geological record of calcified bacterial-algal mats and biofilms. Sedimentology 47, 179–214.
Riding, R., 2008. Abiogenic, microbial and hybrid authigenic carbonate crusts: Components of Precambrian stromatolites. Geologia Croatica 61, 73–103.
Riding, R., Virgone, A., 2020. Hybrid carbonates: in situ abiotic, microbial and skeletal co-precipitates. Earth-Science Reviews 208, 103300.
Riding, R., Fralick, P., Liang, L.Y., 2014. Identification of an Archean marine oxygen oasis. Precambrian Research 251, 232–237.
Rividi, N., van Zuilen, M., Philippot, P., Ménez, B., Godard, G., Poidatz, E., 2010. Calibration of carbonate composition using micro-Raman analysis: application to planetary surface exploration. Astrobiology 10, 293309.
Rouillard, J., García-Ruiz, J.-M., Gong, J., van Zuilen, M.A., 2018. A morphogram for silica-witherite biomorphs and its application to microfossil identification in the early earth rock record. Geobiology 16, 279–296.
Rouillard, J., García-Ruiz, J.-M., Kah, L., Gérard, E., Barrier, L., Nabhan, S., Gong, J., van Zuilen, M.A. 2020. Identifying microbial life in rocks: Insights from population morphometry. Geobiology 18, 282–305.
Russo, F., Neri, C., Mastandrea, A., Baracca, A., 1997. The mud-mound nature of the Cassian platform margins of Dolomites. A case history: the Cipit Boulders from Punta Grohmann (Sasso Piatto Massif, Northern Italy). Facies 36, 25–36.
Russo, F., Mastandrea, A., Stefani, M., Neri, C., 2000. Carbonate facies dominated by syndepositional cements: a key component of Middle Triassic platforms. The Marmolada case history (Dolomites, Italy). Facies 42, 211–226.

Semikhatov, M.A., Gebelein, C.D., Cloud, P., Awramik, S.M., Benmore, W.C. 1979. Stromatolite morphogenesis progress and problems. Canadian Journal of Earth Sciences 19, 992–1015.

Schopf, J.W., 1992. Paleobiology of the Archean. In: Schopf, J.W., Klein, C. (eds), The Proterozoic Biosphere, a Multidisciplinary Study. Cambridge University Press, NY, pp. 25–39.

Schopf, J.W., Packer, M.B., 1987. Early Archean (3.3-billion to 3.5-billion-year-old) microfossils from Warrawoona Group, Australia. Science 237, 70–73.

Schopf, J.W., Sovietov, Y.K., 1976. Microfossils in conophyton from the Soviet Union and their bearing on Precambrian biostratigraphy. Science 193, 143-146.

Schopf, J.W., Kudryavtsev, A.B., Czaja, A.D., Tripathi, A.B., 2007. Evidence of Archean life: Stromatolites and microfossils: Precambrian Research 158, 141–155.

Seong-Joo, L., Golubic, S., 1998. Multi-trichomous cyanobacterial microfossils from the Mesoproterozoic Gaoyuzhuang Formation, China: paleoecological and taxonomic implications. Lethaia 31, 169–184.

Seong-Joo, L., Golubic, S., 1999. Microfossil populations in the context of synsedimentary micrite deposition and acicular carbonate precipitation: Mesoproterozoic Gaoyuzhuang Formation, China. Precambrian Research 96, 183–208

Sergeev, V.N., Knoll, A.H., Grotzinger, J.P., 1995. Paleobiology of the Mesoproterozoic Billyakh Group, Anabar Uplift, northern Siberia. The Paleontological Society, Memoir 69, 1–37.

Shapiro, R.S., 2000. A comment on the systematic confusion of thrombolites. Palaios 15, 166–169.

She, Z.B., Strother, P., Papineau, D., 2014. Terminal Proterozoic cyanobacterial blooms and phosphogenesis documented by the Doushantuo granular phosphorites II: Microbial diversity and C isotopes. Precambrian Research 251, 62–79.

Shi, X.Y., Jiang, G.Q., 2011. Precambrian geobiology and evolution of the Earth surface systems: Co-evolution of early life and environments. In: Xie, S.C., Yin, H.F., Shi, X.Y., (eds), Geobiology: Interaction and Co-evolution of Life and Earth Environment. Science Press, Beijing, pp. 190–235.

Shi, X.Y., Zhang, C.H., Jiang, G.Q., Liu, J., Wang, Y., Liu, D.B., 2008. Microbial mats in the Mesoproterozoic carbonates of the north China Platform and their potential for hydrocarbon generation. Journal of China University of Geosciences 19, 549–566.

Su, W.B., Li, H.K., Huff, W.D., Ettensohn, F.R., Zhang, S.H., Zhou, H.Y., Wan, Y.S., 2010. SHRIMP U-Pb dating for a K-bentonite bed in the Tieling Formation, North China. China Science Bulltin 55, 3312–3323.

Tang, D.J., Shi, X.Y., Pei, Y.P., Jiang, G.Q., Zhao, G.S., 2011. Redox status of the Mesoproterozoic epeiric sea in North China. Journal of Palaeogeography 13, 563–580.

940 Tang, D.J., Shi, X.Y., Jiang, G.Q., 2013a. Mesoproterozoic biogenic thrombolites
941 from the North China platform. International Journal of Earth Sciences 102,
942 401–413.
943 Tang, D.J., Shi, X.Y., Jiang, G.Q., Zhang, W.H., 2013b. Microfabrics in
944 Mesoproterozoic microdigitate stromatolites: evidence of biogenicity and
945 organomineralization at micron and nanometer scales. Palaios 28, 178–194.
946 Tosti, F., Riding, R., 2017 Fine-grained agglutinated elongate columnar stromatolites:
947 Tieling Formation, ca 1420 Ma, North China. Sedimentology 64, 871–902.
948 Tu, C.Y., Chen, Z.Q., Retallack, G.J., Huang, Y.G., Fang, Y.H., 2016. Proliferation of
949 MISS related microbial mats following the end-Permian mass extinction in
950 terrestrial ecosystems: evidence from the Lower Triassic of the Yiyang area,
951 Henan Province, North China. Sedimentary Geology 333, 50–69.
952 Van Lith, Y., Warthmann, R., Vasconcelos, C., Mckenzie, J.A., 2003. Microbial
953 fossilization in carbonate sediments: a result of the bacterial surface involvement
954 in dolomite precipitation. Sedimentology 50, 237–245.
955 Vasconcelos, C., Mckenzie, J.A., 1997. Microbial mediation of modern dolomite
956 precipitation and diagenesis under anoxic conditions (Lagoa Vermelha, Rio de
957 Janeiro, Brazil). Journal of Sedimentary Research 67, 378–390.
958 Vasconcelos, C., Mckenzie, J.A., Bernasconi, S., Grujic, D., Tien, A.J., 1995.
959 Microbial mediation as a possible mechanism for natural dolomite formation at
960 low temperature. Nature 377, 220–222.
961 Wan, B., Windley, B.F., Xiao, W.J., Feng, J.Y., Zhang, J., 2015. Paleoproterozoic
962 high-pressure metamorphism in the northern North China Craton and
963 implications for the Nuna supercontinent. Nature Communications 6, 8344.
964 Wang, T., Feng, Q.L., Huang, Y.F., 2021. Fossil evidence provides new insights into
965 the origin of the Mesoproterozoic ministromatolites. Precambrian Research 336,
966 106426.
967 Wu, S.Q., Chen, Z.Q., Fang, Y.H., Pei, Y., Yang, H., Ogg, J., 2017. A
968 Permian-Triassic boundary microbialite deposit from the eastern Yangtze
969 Platform (Jiangxi Province, South China): Geobiologic features, ecosystem
970 composition and redox conditions. Palaeogeography, Palaeoclimatology,
971 Palaeoecology 486, 58–73.
972 Xu, Y.L., Chen, Z.Q., Feng, X.Q., Wu, S.Q., Shi, G.R., Tu, C.Y., 2017. Proliferation
973 of MISSrelated microbial mats following the end-Permian mass extinction in the
974 northern Paleo-Tethys: evidence from southern Qilianshan region, western China.
975 Palaeogeography, Palaeoclimatology, Palaeoecology 474, 198–213.
976 Yang, H., Chen, Z.Q., Fang, Y.H., 2017. Microbially induced sedimentary structures
977 from the 1.64 Ga Chuanlinggou Formation, Jixian, North China.
978 Palaeogeography, Palaeoclimatology, Palaeoecology 474, 7–25.
979 Yang, H., Chen, Z.Q., Kershaw, S., Liao, W., Lu, A., Huang, Y.G., 2019. Small
980 microbialites from the basal Triassic mudstone (Tieshikou, Jiangxi, South China):
981 Geobiologic features, biogenicity, and paleoenvironmental implications.
982 Palaeogeography, Palaeoclimatology, Palaeoecology 519, 221–235.

Zhang, Y., 1981. Precambrian microfossils from the Sinian of South China. Nature 289, 792–793.

Zhang, Y., 1984. A gunflint type of microfossil assemblage from early Proterozoic stromatolitic cherts in China. Nature 309, 547–549.

Zhang, Y., 1985. Stromatolite mirobiota from the middle Proterozoic Wumishan Formation (Jixian Group) of the Ming Tombs, Beijing, China. Precambrian Research 30, 277–302.

Zhao, C., Shi, M., Feng, Q., Ye, Y., Khan, M.Z., Feng, F., 2020. New study of microbial mats from the Mesoproterozoic Jixian Group, North China: Evidence for photosynthesis and oxygen release. Precambrian Research 344, 105734.

Zhou, H.R., Mei, M.X., Du, B.M., Luo, Z.Q., Lu, M., 2006. Study on the sedimentary features of high frequency cyclothems of the Wumishan Formation at Jixian, Tianjin. Geoscience 20, 209–215.

Zhu, S.X., 1982. An outline of studies on the Precambrian stromatolites of China. Precambrian Research 18, 367–396.

Zhu, S.X., Liang, Y., 1993. On the Proterozoic stromatolites of China. In: Zhu, S. (Ed.), The Stromatolites of China. Tianjin University Press, Tianjin, pp. 3–13.

Zhu, S.X., Cao, R., Zhao, W., Lian, G.Y., 1978. An outline of the stromatolites from the stratotype section of Sinian Suberathem in Chihsien (Jixian) County, North China. Acta Geologica Sinica 52, 209–221.

Zhu, S.X., Xing, Y.S., Zhang, P.Y., 1994. Biostratigraphic Sequence of the Middle-Upper Proterozoic in North-China Platform. Beijing: Geological Publishing House, 1–232.

Figure captions

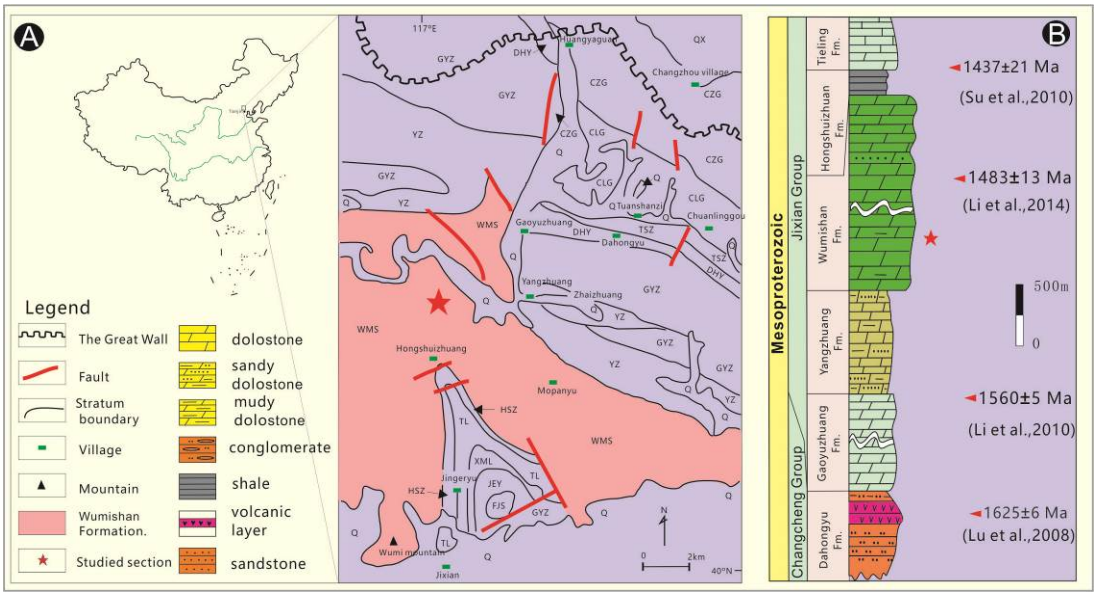

Fig. 1. A, Geological map of the Jixian area, Tianjin City, North China showing distributions of Proterozoic rocks and location of the studied Mopanyu section in Jixian County, Tianjin City. B, Integrating lithostratigraphy and chronostratigraphy of the Meosoproterozoic succession exposed in the Jixian area showing the horizon of stromatolite and U-Pb zircon radiometric ages (geological map after Mei et al., 2008). Abbreviations of stratigraphic units: Q = modern loose sediments, FJS = Fujunshan Formation, JEY = Jingeryu Formation, XML = Xiamaling Formation, TL = Tieling Formation, HSZ = Hongshuizhuang Formation, WMS = Wumishan Formation, YZ = Yangzhuang Formation, GYZ = Gaoyuzhuang Formation, DHY = Dahongyu Formation, TSZ = Tuanshanzi Formation, CLG = Chuanlinggou Formation, CZG = Changzhougou Formation, QX = Qianxi Group of the Archean-Paleoproterozoic metamorphic basement.

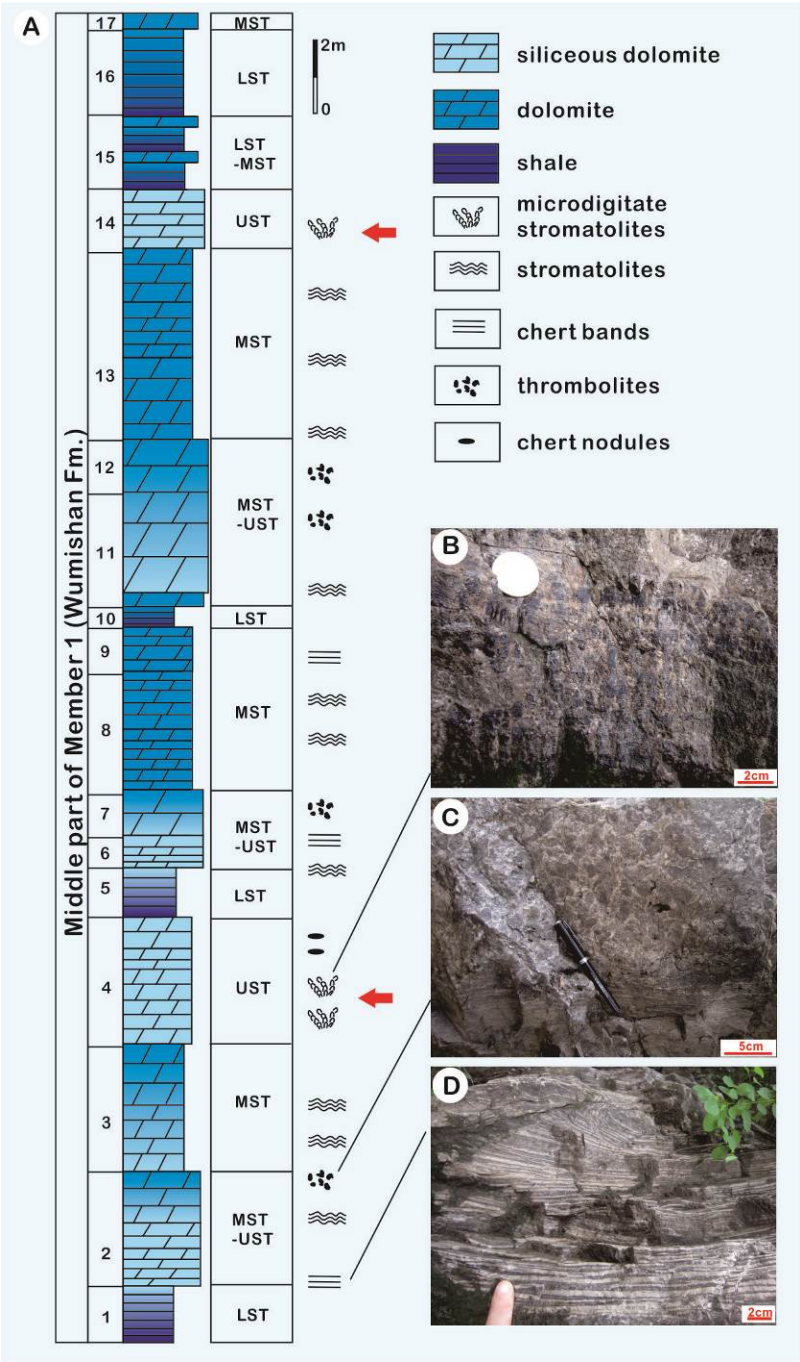

Fig. 2. Composite stratigraphy, microfacies features and palaeoenvironmental interpretations of the middle part of Member 1 (Wumishan Formation) in the the Mopanyu section of Jixian County, Tianjin City, North China. A, Lithostratigraphy, microfacies and palaeoenvironmental settings. LST = lower part of subtidal zone, MST = middle part of subtital zone, UST = upper part of subtidal zone. B, Field photo showing microdigitate dolomitic stromatolites with mostly non-branching columns (the coin is 2.5 cm in diameter). C, Field photo of thrombolites yielded from dolomites showing mottled textures (the pen is 15 cm long). D, Field photo showing alternations of millimeter- to centimeter-thick black and white chert bands with flat to slightly convoluted laminations.

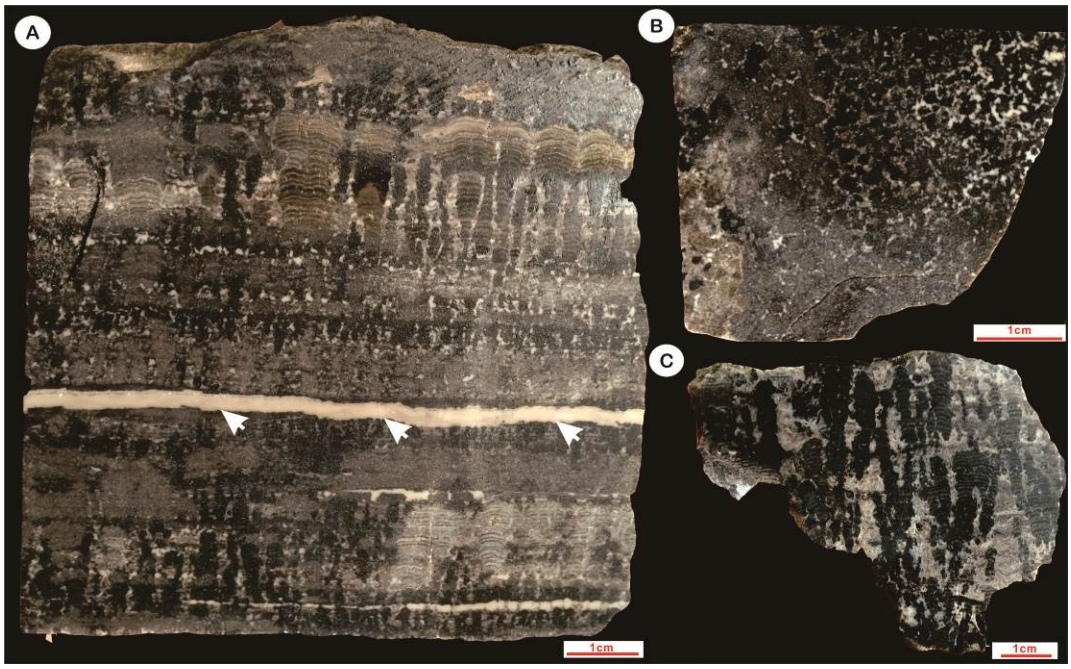

Fig. 3. Polished slab of the Wumishan stromatolites. A, Polished slab in cross-sectional view showing digitate to microdigitate, low-relief columns of stromatolites, dolomitic wackestone (white arrows). B, Polished slab of a planar view of an MDS bed showing circular, domal outlines of stromatolite columns. C, Polished slab in cross-sectional view showing digitate, branching and non-branching columns of microdigitate stromatolites.

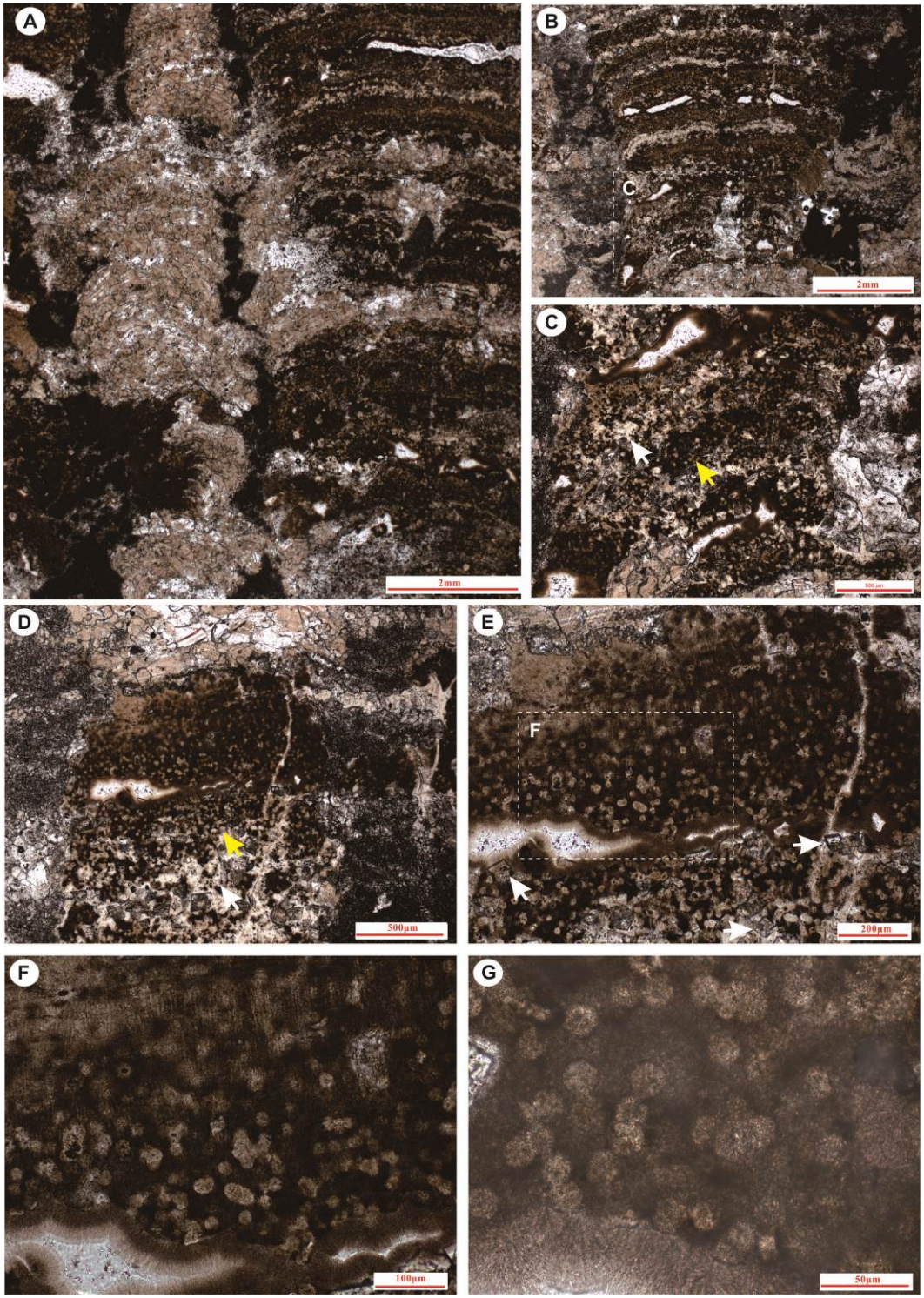

Fig. 4. Photomicrographs of the Wumishan MDSs. A, B, Digitate columns branching and merging occasionally with laminae being destructed occasionally by cavities that are filled with calcite. C, Close-up of B, digitate columns showing distinct alternations of light coloured (white) and dark coloured (yellow) laminae. D, Digitate columns showing distinct alternations of light coloured (white) and dark coloured (yellow) laminae, flanked with dark coloured interspaces between columns (arrows) filled with spheroids or stromatolite fragments. E, showing dark coloured laminae that contain aggregates of spheroids and some small cavities filled with outsized dolomite

crystals (arrows). F, Close-up of E showing dark coloured laminae that contain aggregates of spheroids and a cavity-like structure lined with botryoidal features near the bottom. G, showing spheroids consortia penetrated by tiny vertically orientated fibrous fabrics.

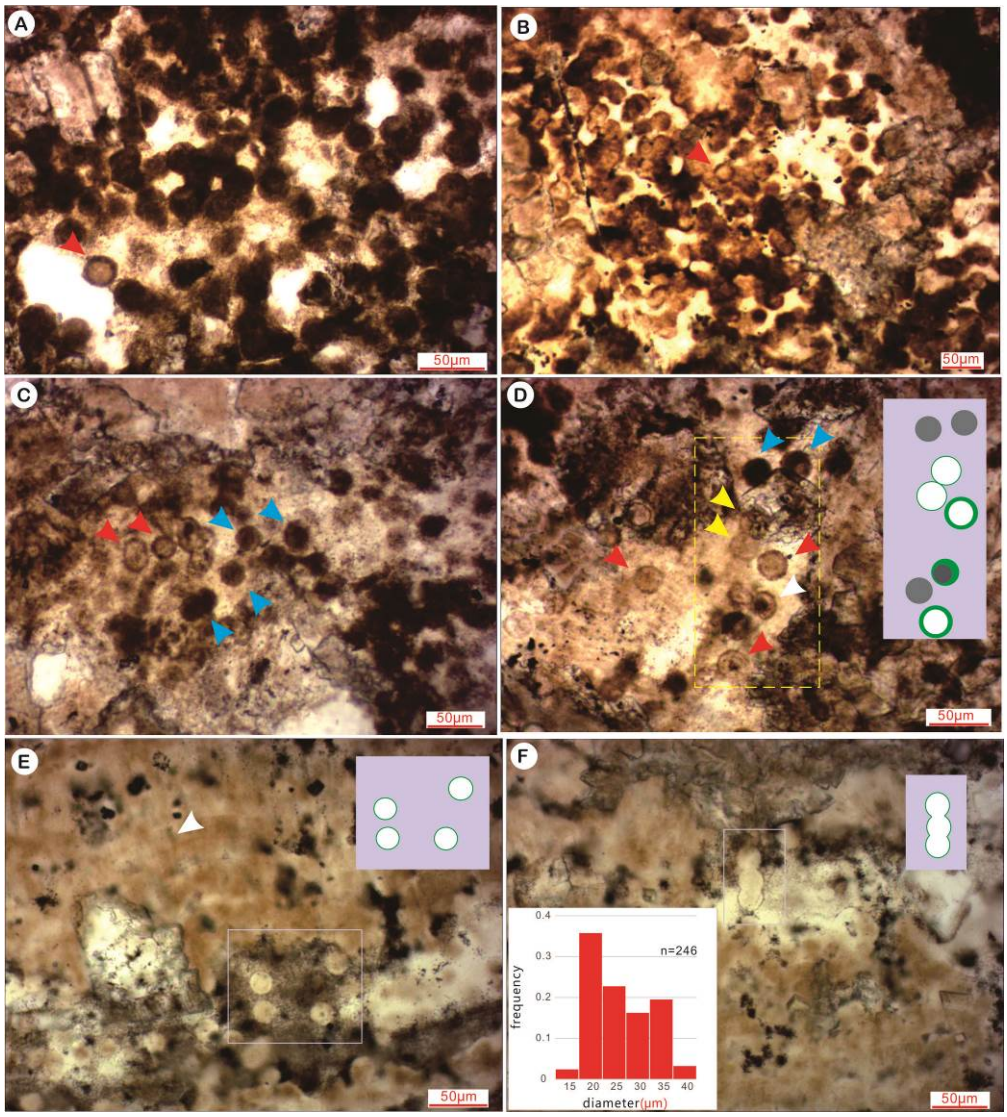

Fig. 5. Photomicrographs of the Wumishan MDSs. Spheroids consortia in dark coloured laminae. Colour arrows stand for different kinds of spheroids. A, B, spheroid with shell-like annulus, red arrows. C, two kinds of spheroids, spheroids with shell-like annulus, red arrows, and brown solid spheroids, blue arrows. D, four type spheroids, light brown hollow spheroids, yellow arrows, spheroids with shell-like annulus amd black core, white arrow, red and blue arrows as described in C. E, brown four light brown hollow spheroids. Fibrous fabrics (brown area) and single fibers (white arrow). F, three concatenated light brown spheroids and, in inset, an histogram of the diameter sizes frequency distribution of 246 individual spheroids measured.

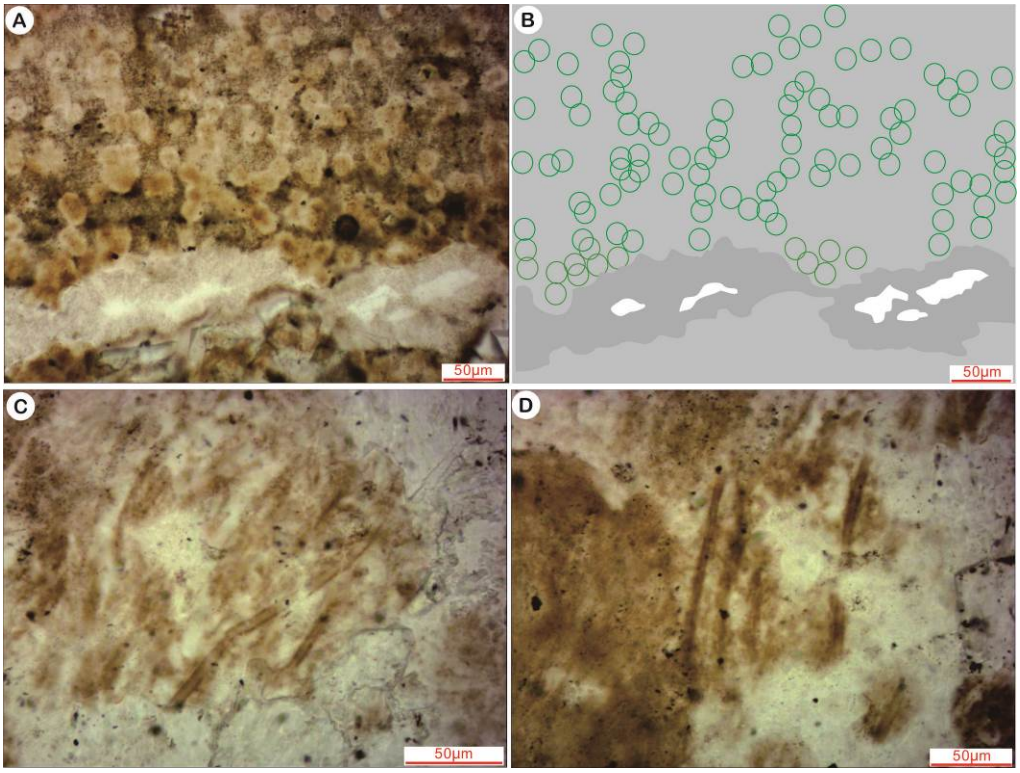

Fig. 6. Photomicrographs of the Wumishan MDSs. A, Spheroids consortia in dark coloured laminae. B, Interpretive cartoon of microscopic spheroids and associated botryoidal features and dolomite rhombs in A. C-D, Slightly curved filaments between the MDS columns that are mostly parallel-aligned and brown in colour due to their composition of organic matter.

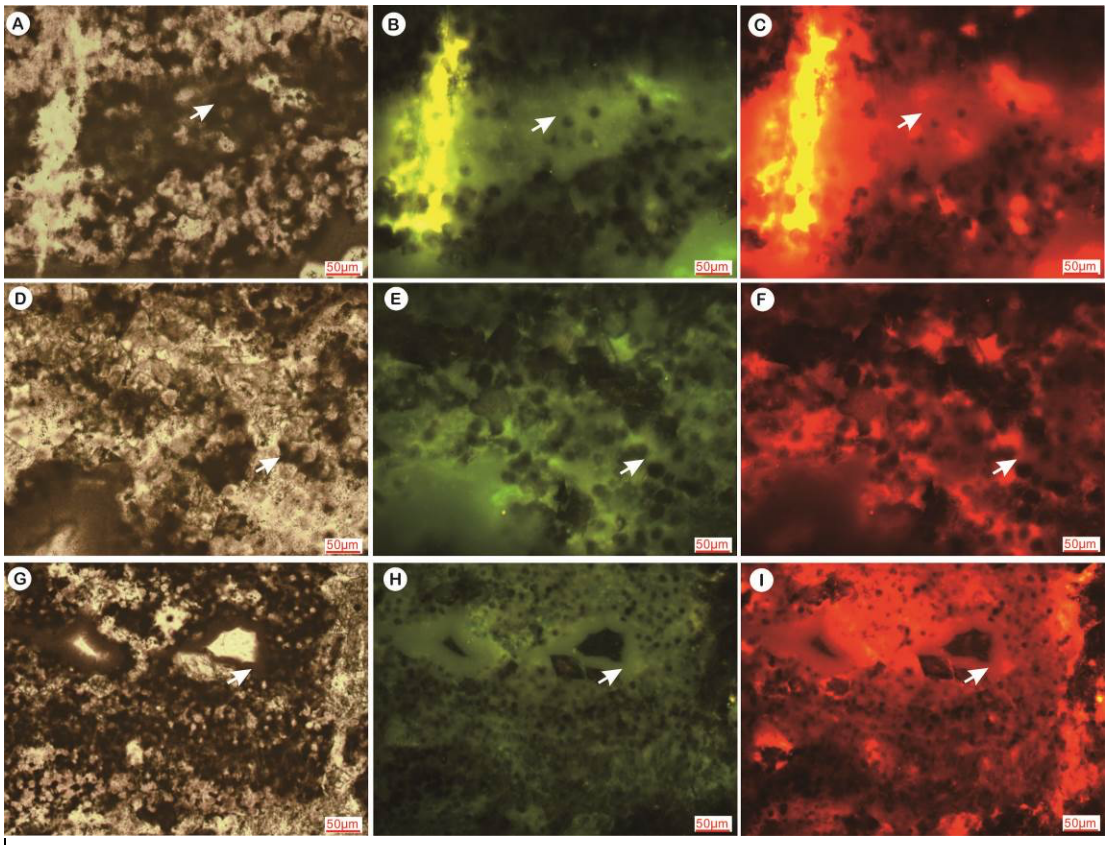

Fig. 7. Polarized microscope and fluorescent images showing coccoid-like spheroid consortia. A, D, G, Polarization microscope images. B, E, H, Fluorescence images (purple fluorescent wavelength 450-490 nm). C, F, I, Fluorescence images (green fluorescent wavelength 510-560 nm). Organic-enriched particles (arrows) show strong fluorescence in both green and red colours. Inside laminae rich in organic matter and microscopic spheroids, note the presence of botryoid-like cavity-structures lined with dense organic matter around cores almost free of of organic matter in G-I.

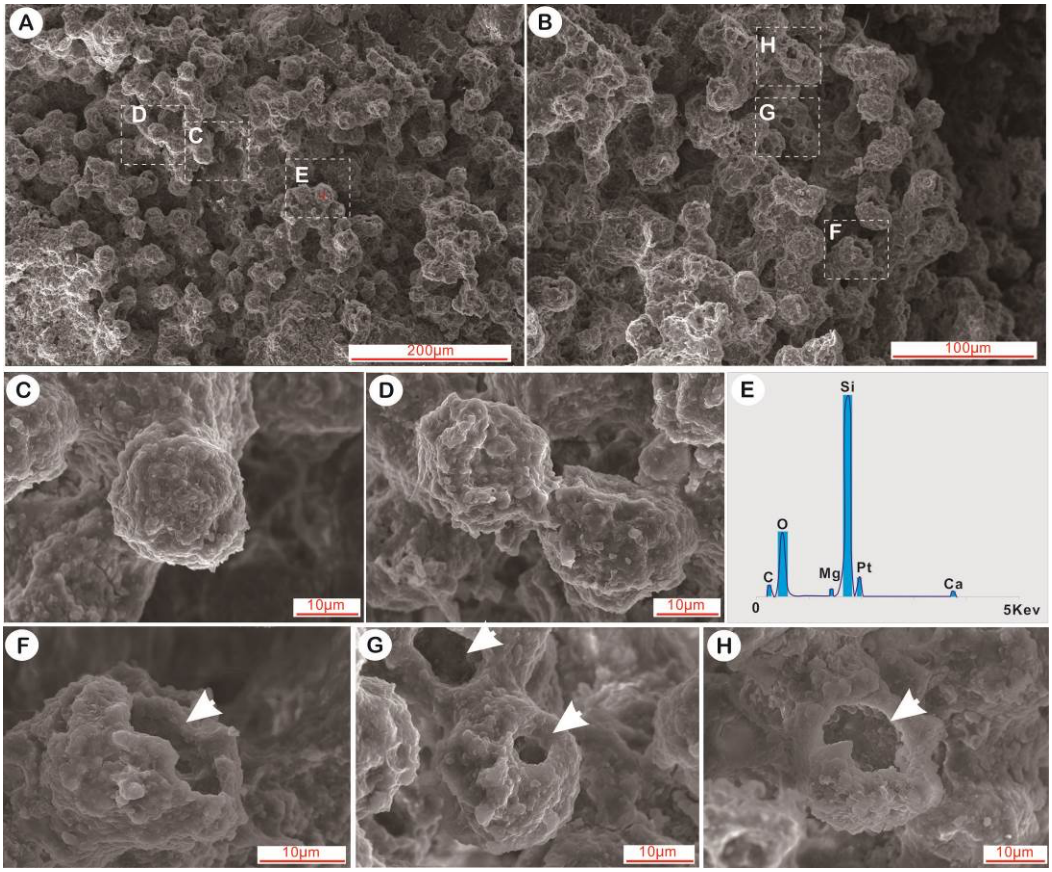

Fig. 8. Secondary electron images of micro-fabrics and aggregates of microscopic spheroid in dark coloured laminae and EDS analytical results of spheroid surface (Natural weathering without acid treatment). A–B, aggregates of spheroids. C, Close-up of boxed area in A showing solitary spheroid having unsmooth surface. D, Close-up of boxed area in A showing paired spheroids with irregular outline and unsmooth surfaces. E, EDS peaks of the crossed point in A showing major components of Si and O, and minor contents of C, Ca and Mg, indicating a replacement of silica due to silicification. F–H, Close-up of boxed area in B, showing solitary spheroid having one broken opening (arrows) on surface.

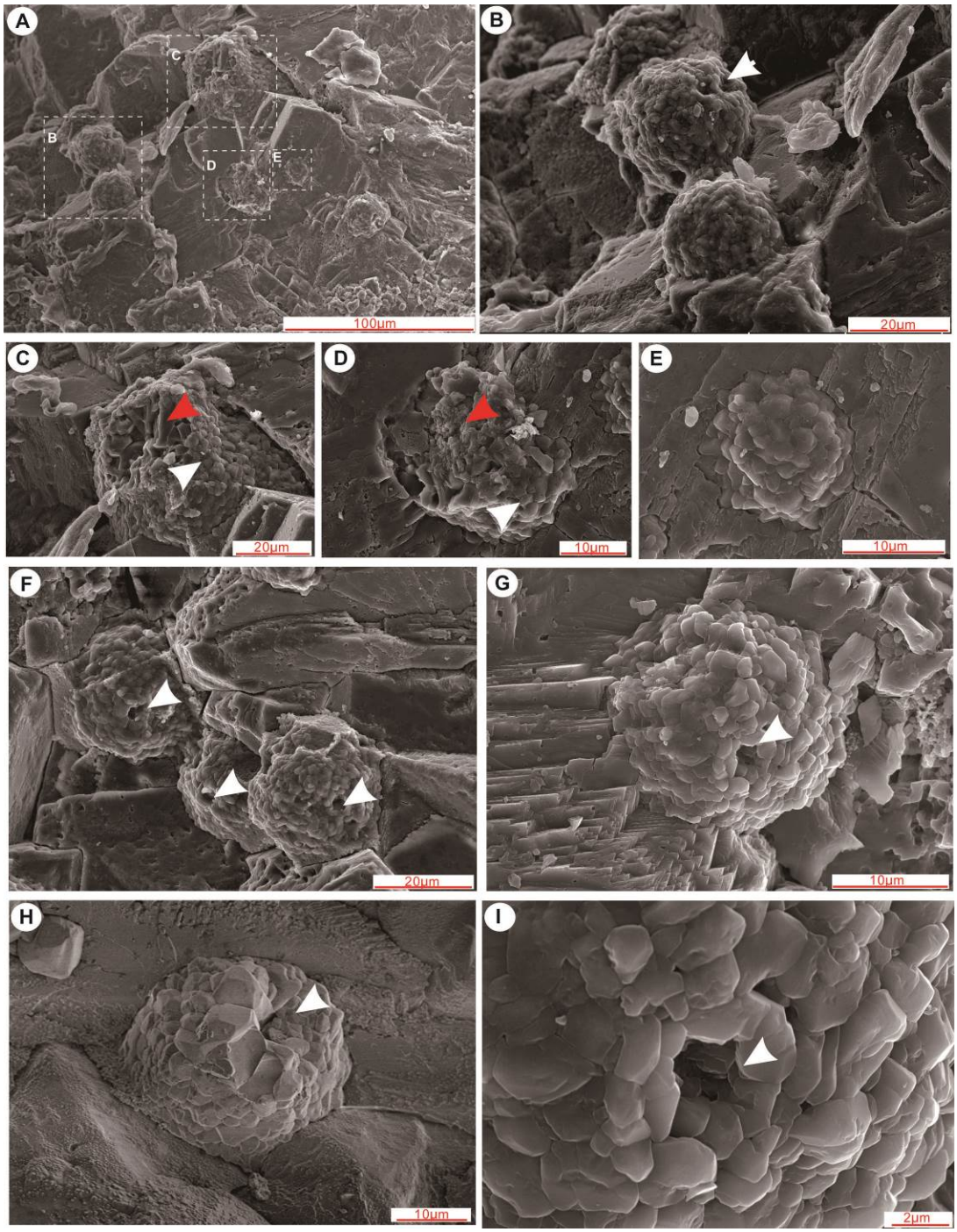

Fig. 9. SEM images of spheroids detected in light coloured laminae. A, Spheroids grew on sparry calcites. B, Close-up of boxed area in A showing three spheroids elevated from sparitic calcite crystals. Note the middle spheroid embraces a distinct rounded opening on surface (arrow). C, Close-up of boxed area in A showing a coarse sparitic crystal calcite nucleus (red arrow) surrounded by a thin layer of micrite envelope (white arrow) in one broken spheroid. D, Close-up of boxed area in A showing a micrite framboidal nucleus (red arrow) surrounded by coarse calcite crystal rims (white arrow) in one broken spheroid that is covered partly by background sparry calcite. E, Close-up of boxed area in A showing one spheroid being covered partly by background sparry calcite with nano-particles on surface. F, Colony of three

coccoid-like spheroids, with each embracing one pronounced circular opening (arrows) and nano-particles on surface. G, Close-up of one spheroid with a distinct rounded opening (arrow) and nano-particles on surface. H, Close-up of one spheroid that is broken around the opening (arrow). I, Close-up of one opening on spheroid surface in G showing rough margins of opening that comprise nano-particles.

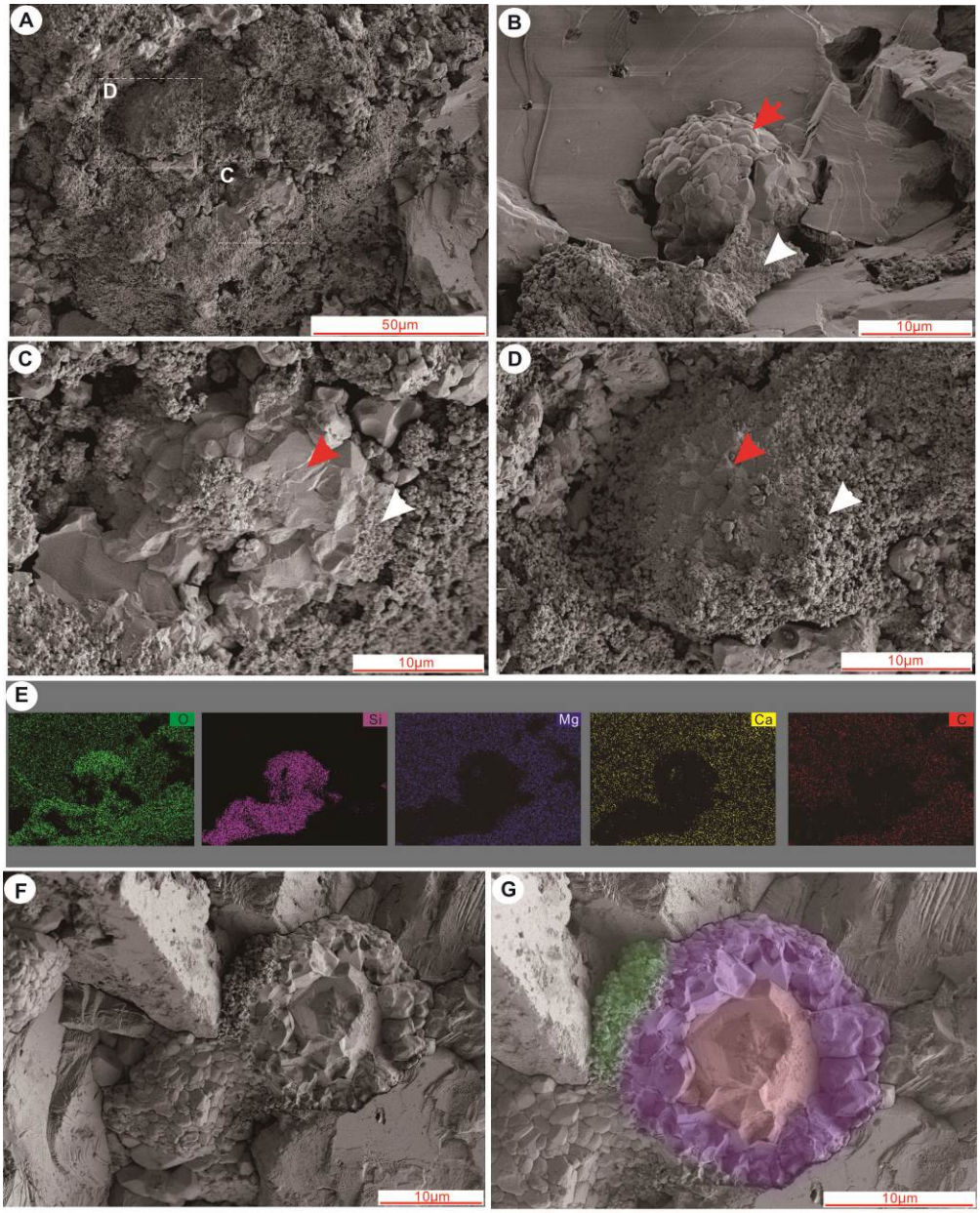

Fig. 10. Secondary electron images and EDS elemental mapping of spheroids from dark colored laminae. A, SEM image showing copious nano-particles covering spheroids and scattering on rocks. B, One complete spheroid growing in background calcite crystals with coarse calcite crystal sheaths on surface. Note that nano-particle aggregates (arrow). C, Close-up of boxed area in A showing that one broken spheroid possesses coarse calcite crystal nucleus (red arrow) surrounded by thin layer of sparitic calcite envelope (white arrow), and is covered partly with micrite sheaths

(nano-particles) . D, Close-up of boxed area in A showing that one spheroid is covered by thick micrite sheaths composed of nano-particles. E, EDS elemental mapping of one spheroid in B showing that Si content is limited to the microscopic spheroid and nano-particles. Oxygen content is high in all phases, whereas Mg, Ca and C content (dolomite) is low in the spheroid and nano-particles, but high in the host matrix. F and G, A broken microscopic spheroid in black and white and with features labelled in various colors, respectively showing a nucleus of coarse calcite (light red) surrounded by thin sheath of coarse sparitic calcite (purple), which are coated with micrite (nano-particles) layers (green).

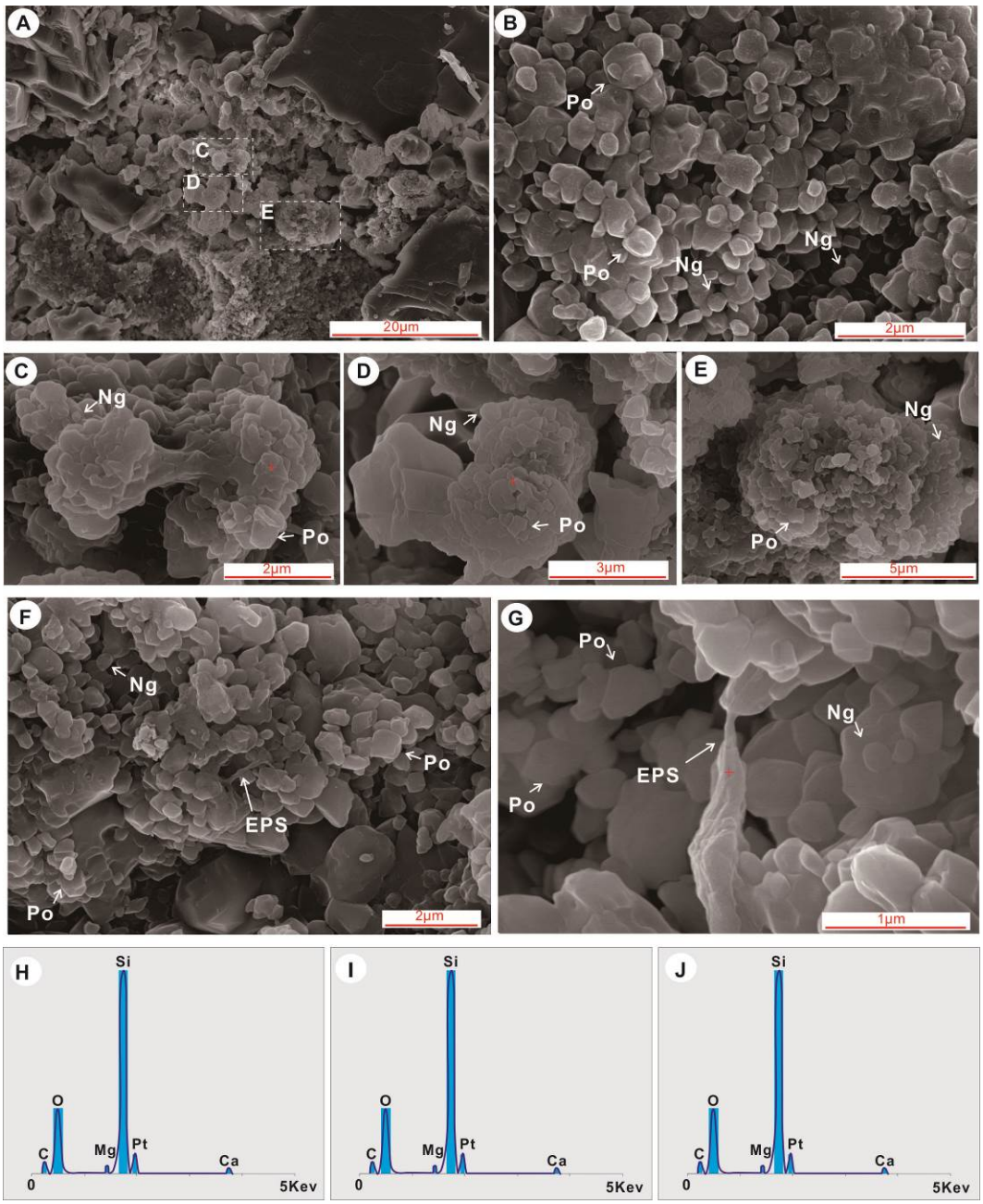

Fig. 11. SEM images of nano-particles, Po = polyhedrons and Ng = nanoglobules. A, Nano-particle aggregates. B, Close-up of nano-particle aggregates showing abundant polyhedrons (Po) and nanoglobules (Ng). C, Close-up of boxed area in A showing

dumbbell-shaped bursts of polyhedrons (Po) and nanoglobules (Ng). D, Close-up of boxed area in A showing primitive form of dumbbell-shaped bursts of polyhedrons (Po) and nanoglobules (Ng) with closely arranged bell-like aggregates. E, Close-up of boxed area in A showing spherical aggregate of polyhedrons (Po) and nanoglobules (Ng). F, Nano-particle aggregates containing abundant filaments and mucuslike films (purported EPS), polyhedrons (Po) and nanoglobules (Ng). G, Close-up of boxed area in F showing filaments and mucuslike films (purported EPS), polyhedrons (Po) and nanoglobules (Ng). H–J, EDS analytical results of crossed points in C, D and G, respectively showing almost same elemental composition patterns of polyhedrons (Po), nanoglobules (Ng), and mucuslike films, respectively.

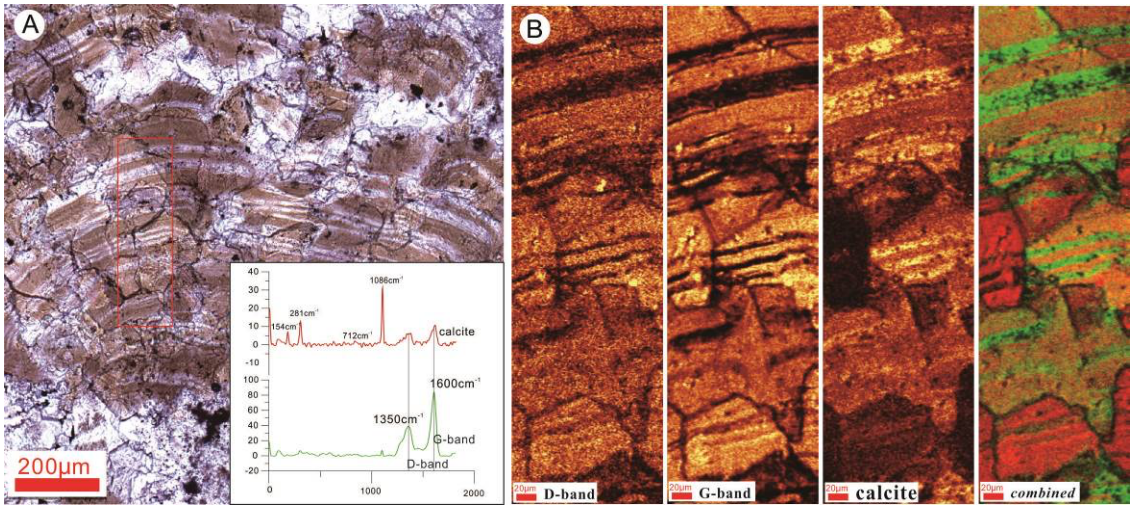

Fig. 12. Optical petrographic images and corresponding Raman maps of areas corresponding to boxed area showing the spatial distribution (recorded by the parameter I-1350 and I-1600) of the organic matter in MDS without spheroids. (A) Transmitted light image of finely laminated domal stromatolite with layers of organic matter (brown) but without microscopic spheroids. (B) Selected Raman images of the laminated dome showing D-band, G-band, calcite, and combined images. Raman spectra for calcite, which shows peaks at 154, 281, 712 and 1086 cm^{-1}, and for organic matter, which shows peaks at 1350 cm^{-1} (D-band) and 1600 cm^{-1} (G-band).

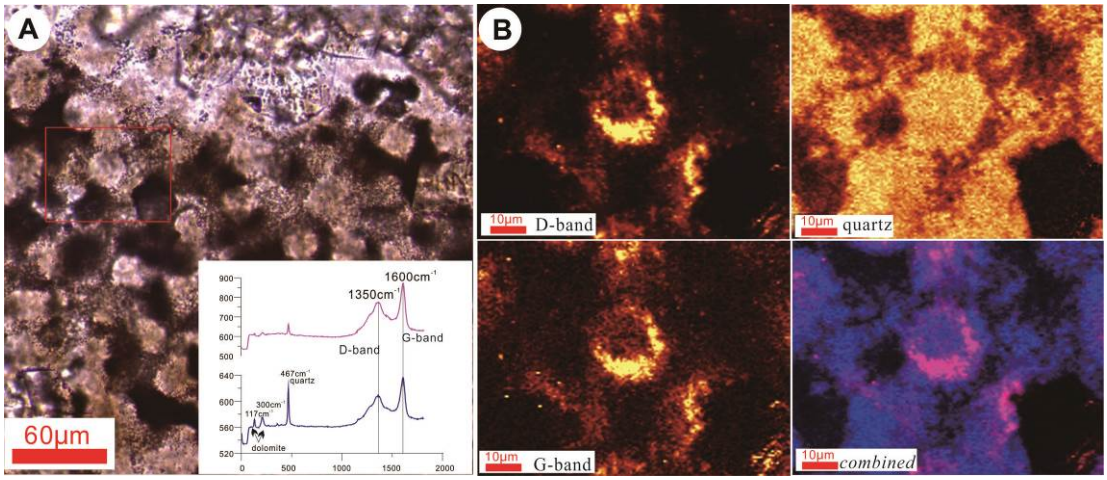

Fig. 13. Optical petrographic images and corresponding Raman maps of boxed area showing the spatial distribution (recorded by the parameter I-1350 and I-1600) of the organic matter in the spheroids laminated dome. (A) Transmitted light image of light-brown spheroids in organic-rich laminae. (B) The Raman spectra obtained in (A), bands at 176 and 299 cm^{-1} that are assigned to dolomite. The peak at 465 cm^{-1} represents microcrystalline quartz, while the peaks for organic matter are centered at 1350 and 1600 cm^{-1}. Selected Raman images of spheroids in organic-rich laminae for the D-band and G-band of organic matter, for quartz, and for the combined hyperspectral image.